

# FastGxC: Fast and Powerful Context-Specific eQTL Mapping in Bulk and Single-Cell Data

Lena Krockenberger<sup>\*\*1</sup>, Andrew Lu<sup>\*\*2</sup>, Mike Thompson<sup>3</sup>, Cuining Liu<sup>1,4</sup>, M Grace Gordon<sup>5</sup>, Amanda Ramste<sup>6,7</sup>, Ivan Carcamo-Orive<sup>8,9</sup>, Joshua W. Knowles<sup>7</sup>, Andy Dahl<sup>10</sup>, Chun Jimmie Ye<sup>11</sup>, Noah Zaitlen<sup>4,12,13</sup>, and Brunilda Balliu<sup>\*12,14,15</sup>

<sup>1</sup>Bioinformatics Interdepartmental Graduate Program, University of California Los Angeles, Los Angeles, CA, USA

<sup>2</sup>UCLA-Caltech Medical Scientist Training Program, David Geffen School of Medicine, University of California Los Angeles, Los Angeles, CA, USA

<sup>3</sup>Systems and Synthetic Biology, Centre for Genomic Regulation, The Barcelona Institute for Science and Technology (BIST), Barcelona, Spain

<sup>4</sup>Department of Human Genetics, University of California Los Angeles, Los Angeles, CA, USA

<sup>5</sup>Biological and Medical Informatics Graduate Program, University of California, San Francisco, San Francisco, CA, USA

<sup>6</sup>Institute for Molecular Medicine Finland (FIMM), HiLIFE, University of Helsinki, Helsinki, Finland

<sup>7</sup>Division of Cardiovascular Medicine, Cardiovascular Institute, Diabetes Research Center, Stanford, CA USA

<sup>8</sup>Department of Endocrinology, Metabolism, Nutrition, and Kidney Disease, Biobizkaia Health Research Institute, Barakaldo, Spain

<sup>9</sup>IKERBASQUE, Basque Foundation for Science, Bilbao, Spain

<sup>10</sup>Section of Genetic Medicine, University of Chicago, Chicago, IL, USA

<sup>11</sup>Division of Rheumatology, Department of Medicine, University of California, San Francisco, San Francisco, CA, USA

<sup>12</sup>Department of Computational Medicine, University of California Los Angeles, Los Angeles, CA, USA

<sup>13</sup>Department of Neurology, University of California Los Angeles, Los Angeles, CA, USA

<sup>14</sup>Department of Pathology and Laboratory Medicine, University of California Los Angeles, Los Angeles, CA, USA

<sup>15</sup>Department of Biostatistics, University of California Los Angeles, Los Angeles, CA, USA

<sup>\*</sup>Corresponding author; email: bballiu@ucla.edu

<sup>\*\*</sup>these authors contributed equally

## 1 Abstract

2 Context-specific eQTLs mediate genetic risk for complex diseases. However, limitations in cur-  
3 rent methods for identifying these eQTLs have hindered their comprehensive characterization and  
4 downstream interpretation of disease-associated variants. Here, we introduce FastGxC, a method  
5 to efficiently and powerfully map context-specific eQTLs by leveraging the correlation structure  
6 in genomic studies with repeated sampling, e.g., single-cell RNA-seq studies. Using simulations,  
7 we demonstrate that FastGxC is up to nine times more powerful and  $10^6$  times faster than exist-  
8 ing approaches, reducing computation time from years to minutes. We applied FastGxC to bulk  
9 multi-tissue (N=698) and single-cell PBMC (N=1,218) RNA-seq datasets, generating comprehen-  
10 sive tissue- and cell-type-specific eQTL maps. These eQTLs exhibited up to four-fold enrichment  
11 in open chromatin regions from matched contexts and were twice as enriched as standard context-  
12 specific eQTLs, highlighting their biological relevance. Furthermore, we examined the relationship  
13 between context-specific eQTLs and complex human traits and diseases. FastGxC improved pre-  
14 cision in identifying relevant contexts for each trait by three-fold and expanded candidate causal  
15 genes by 25% in cell types and 6% in tissues compared to standard eQTLs. In summary, FastGxC  
16 provides a powerful framework for mapping context-specific eQTLs, advancing our understanding  
17 of gene regulatory mechanisms underlying complex human traits and diseases.

## 18 1 Introduction

19 Over the past 15 years, genome-wide association studies (GWAS) have identified tens of thousands  
20 of genetic variants linked to complex traits and diseases [1]. A majority of these variants reside in  
21 non-coding regions, often overlapping DNA regulatory elements [2], which suggests their functional  
22 effects are mediated through transcriptional regulation [2–5]. This observation has driven significant  
23 efforts to identify expression quantitative trait loci (eQTLs) — genetic variants associated with  
24 gene expression changes — and use them to link GWAS variants to their regulatory targets [6–  
25 [15]. Despite these efforts, only 21% of GWAS variants, on average per trait, overlap with known  
26 cis eQTLs from bulk tissues [12], underscoring a persistent gap between genetic associations and

27 regulatory function [16–18].

28 A key factor for this missing regulation is the context-specific nature of many disease-relevant  
29 eQTLs [16, 18], which often appear only in specific tissues [12], cell types [10, 14, 15], or environ-  
30 mental conditions [19–23], making them difficult to detect. In contrast, broadly shared eQTLs,  
31 while easier to detect, are less enriched for GWAS variants [12, 14], likely due to negative selec-  
32 tion [16, 18]. Another major factor is that many bulk [8, 12] and all single cell RNA-Sequencing  
33 (RNA-Seq) studies rely on repeated sampling, where the same donor provides samples across mul-  
34 tiple contexts. While this design minimizes experimental variability, it introduces intra-individual  
35 correlation, which, if unaccounted for, inflates type I error rate to identify an eQTL and reduces  
36 the power to test if the eQTL is context-specific.

37 Several methods have been developed to identify context-specific eQTLs in studies with re-  
38 peated sampling (see Table S1). These methods fall into two broad categories. The first comprises  
39 approaches that jointly analyze data across contexts and test for context-specific eQTLs by incor-  
40 porating a genotype-by-context (GxC) interaction term. Note that, while we refer to eQTLs with  
41 significant GxC effects as context-specific, in alignment with common genomics terminology [24,  
42 25], the more precise term would be context-dependent eQTLs. This includes (generalized) linear  
43 mixed model (LMM)-based methods [24–29], which model the GxC effect linearly, and methods  
44 that capture non-linear GxC effects [30]. To account for repeated measurements, these methods  
45 include a random effect for the individual or cell. While powerful, their mixed model framework  
46 makes them computationally intensive for large eQTL studies. This challenge is particularly ex-  
47 acerbated when modeling all cell types jointly. Additionally, some of these methods [24, 30] infer  
48 latent cellular contexts, further increasing computational costs.

49 The other category includes methods that follow a two-step process: first, they map eQTLs  
50 separately in each context (context-by-context; CxC), then they define context-specificity by post  
51 hoc examination of eQTL summary statistics across contexts [10, 12, 15, 31–33]. While CxC  
52 approaches are fast, particularly those developed for (pseudo)-bulk data [10, 12, 15, 33], they have  
53 major limitations. First, CxC approaches can be significantly underpowered because they do not  
54 fully leverage all available data. Second, many rely on ad hoc definitions of context-specificity based  
55 on subjective thresholds of effect size differences between contexts [33, 34] or the significance of an

56 eQTL in a single context [10, 12, 15]. These definitions can lead to both false-positive context-  
57 specificity (e.g., when effects in certain contexts fail to reach significance due to chance or uneven  
58 power across contexts) and false-negative context-specificity (e.g., when an eQTL is shared across  
59 contexts but still shows GxC interaction effects). Taken together, these limitations constrain the  
60 interpretation of disease-associated variants, as current methods fail to fully capture the complexity  
61 of context-specific regulatory variation.

62 To address these challenges, we introduce FastGxC, a novel method that efficiently maps  
63 context-specific eQTLs while accounting for repeated sampling. In brief, FastGxC decomposes  
64 gene expression into context-shared and context-specific components and estimates genetic effects  
65 on these components using linear regression. We show analytically and empirically that FastGxC's  
66 eQTL effect estimates can be viewed as computationally efficient reparametrizations of those ob-  
67 tained through CxC and LMM-GxC approaches. FastGxC has several key advantages over previous  
68 methods. First, it directly maps specific eQTLs without the need for post hoc analyses or arbitrary  
69 thresholds. Second, by accounting for intra-individual correlation, it adjusts for background noise  
70 and confounding factors unrelated to the context of interest, e.g., sex, age, population stratification,  
71 or sequencing batch [35-37], maximizing power to detect context-specific eQTLs (Figure S1). Third,  
72 FastGxC leverages ultra-fast implementations of linear regression models, similar to those used in  
73 CxC eQTL mapping approaches [38-40], which reduce computational time from years to minutes.  
74 FastGxC can work on any continuous molecular phenotype and its output integrates naturally with  
75 methods developed to improve the statistical power of eQTL mapping, such as mash [34].

76 We first show in simulations that FastGxC is as powerful as the LMM-GxC approaches but  
77 orders of magnitude faster. Both approaches significantly outperform CxC-based methods to map  
78 context-specific eQTLs. We then applied FastGxC to multi-tissue bulk RNA-Seq data from the  
79 GTEx Consortium [12] (N=698 individuals) and single-cell peripheral blood mononuclear (PBMC)  
80 RNA-Seq data from the CLUES [14] (N = 237) and OneK1K [15] (N = 981) cohorts, which we  
81 meta-analyze, to produce comprehensive tissue- and cell type-specific eQTL maps across 49 tissues  
82 and 8 PBMC cell types. FastGxC context-specific eQTLs show up to four-fold enrichment in open  
83 chromatin regions from matched contexts and are twice as enriched as standard context-specific  
84 eQTLs, highlighting their biological relevance. We further examine their relationship with complex

85 traits and diseases, showing that FastGxC eQTLs improve precision in identifying relevant GWAS  
86 contexts by three-fold and expand candidate causal genes by 25% in cell types and 6% in tissues  
87 compared to standard eQTLs. In addition, FastGxC context-specific eQTLs show a 1.2-fold in-  
88 crease in colocalization with complex traits compared to shared eQTLs, providing evidence that  
89 context-specific regulation helps explain regulatory mechanisms of complex diseases that remain  
90 unaccounted for by shared eQTLs. In summary, FastGxC provides a powerful framework for con-  
91 structing context-specific eQTL maps, offering key insights into the gene regulatory mechanisms  
92 underlying complex human diseases.

## 93 2 Results

94 **FastGxC method overview.** We illustrate the FastGxC method using tissues as contexts (Figure 95 1A), but the method can be applied to any set of discrete contexts, for example, cell types 10, 96 14, 15 or environmental stimuli, sampled across overlapping individuals. FastGxC works in three 97 steps. First, for each individual  $i$  ( $i = 1, \dots, N$ ) and context  $c$  ( $c = 1, \dots, C$ ), FastGxC decomposes 98 the expression of each gene ( $E_{ic}$ ) into two components: a shared component ( $E_i^{sh}$ ), representing the 99 average expression across contexts, and a context-specific component ( $E_{ic}^{sp}$ ), representing the resid- 100 ual expression in the contexts after subtracting the shared component (Figure 1A - Decomposition 101 step), i.e.,  $E_{ic} = E_i^{sh} - E_{ic}^{sp}$ . This decomposition, analogous to repeated-measures ANOVA, removes 102 shared eQTLs effects and shared noise from the context-specific components, thereby increasing 103 power to detect context-specific eQTLs (Figure S1) 41.

104 Next, for each gene-cis-SNP pair, FastGxC estimates a shared eQTL effect ( $\beta^{sh}$ ) and  $C$  spe- 105 cific eQTL effects ( $\beta_1^{sp}, \dots, \beta_C^{sp}$ ) by regressing the genotype at the cis-SNP on the shared expression 106 component and each of the  $C$  context-specific components (Figure 1A - eQTL mapping step). This 107 step employs ultra-fast implementations of linear regression models optimized for eQTL mapping 108 38, 39, enabling computational efficiency comparable to standard eQTL mapping methods. The 109 shared and context-specific effects represent a reparametrization of the eQTL effects obtained from 110 conventional context-by-context eQTL mapping ( $\beta_1, \dots, \beta_C$ ) (Figure 1B and S16). Specifically, the 111 shared effect corresponds to the mean eQTL effect size across contexts, i.e.,  $\beta^{sh} = \frac{1}{C} \sum_{c=1}^C \beta_c$ ,

112 while the context-specific effects capture the residual eQTL effects in each context after account-  
113 ing for the shared effect, i.e.,  $\beta_c^{sp} = \beta_c - \beta^{sh}$ ,  $\forall c \in \{1, \dots, C\}$ . This decomposition separates  
114 the pleiotropic (shared) effect of an eQTL across all contexts from the context-specific effects, en-  
115 abling clearer interpretation of context-specific genetic effects. Because CxC itself can be viewed  
116 as a reparametrization of the LMM-GxC framework, FastGxC provides a computationally efficient  
117 reparametrization of LMM-GxC. Full details of the analytical derivation are provided in the Online  
118 Methods and Supplementary Text.

119 Finally, to account for multiple testing across genes, SNPs, and contexts, FastGxC employs the  
120 hierarchical False Discovery Rate (FDR)-controlling procedure implemented in [42] (Online Methods  
121 and Figure S2). FastGxC defines a gene-SNP pair as an eQTL if the SNP has a significant effect on  
122 the shared or any of the specific components of gene expression, i.e., if the global null hypothesis  
123  $H_0 : \beta^{sh} = \beta_1^{sp} = \beta_2^{sp} = \dots = \beta_C^{sp} = 0$  is rejected. If an eQTL is detected, FastGxC defines a  
124 context-specific eQTL as a SNP with a significant effect on at least one of the specific components  
125 of expression of the gene, i.e., if the global null hypothesis  $H_0^{sp} : \beta_1^{sp} = \beta_2^{sp} = \dots = \beta_C^{sp} = 0$  is rejected.  
126 This global test directly identifies context-specific eQTLs, eliminating the need for post hoc analyses  
127 or arbitrary thresholds. Finally, if significant eQTL effect size heterogeneity is detected, FastGxC  
128 conducts  $C$  marginal tests to determine the specific context(s) driving the observed heterogeneity,  
129 i.e.,  $H_0^c : \beta_c^{sp} = 0 \quad \forall c \in 1, \dots, C$ . Note that these tests do not specifically flag the contexts with  
130 non-zero eQTL effects; rather, they detect contexts whose effect sizes deviate significantly from the  
131 shared effect. To illustrate how FastGxC identifies different patterns of context-specificity, Figure  
132 1B shows toy examples of eQTLs with varying patterns of effects across contexts.

133 The first two panels (“No Heterogeneity”) depict scenarios under the null hypothesis of no  
134 eQTL effect size heterogeneity across contexts, with either a shared eQTL effect (“Shared”) or no  
135 shared eQTL effect (“No Shared”). FastGxC does not classify either of these eQTLs as context-  
136 specific, as there is no significant heterogeneity of their effects across contexts, but it would classify  
137 the second scenario as a (shared) eQTL. The remaining panels illustrate scenarios under the al-  
138 ternative hypothesis of eQTL effect size heterogeneity. These include heterogeneity driven by a  
139 single context (“Single-context Heterogeneity”) or heterogeneity spanning all contexts (“Extensive  
140 Heterogeneity”). FastGxC identifies all these scenarios as context-specific eQTLs, irrespective of

141 the presence of a shared eQTL effect. By contrast, the commonly used CxC approach defines  
142 context-specific eQTLs as variants with significant eQTL effects in only a single context. As a re-  
143 sult, this approach would classify only the first alternative scenario (“Single-context Heterogeneity  
144 - No Shared”) as a context-specific eQTL and would overlook more complex patterns of hetero-  
145 geneity, such as cases where heterogeneity exists alongside a shared effect or where heterogeneity is  
146 distributed across multiple contexts, highlighting its limitations compared to FastGxC.

147 **FastGxC outperforms existing methods in simulation studies.** We used a series of sim-  
148 ulated scenarios to evaluate the performance of FastGxC to detect an eQTL and determine if the  
149 eQTL effect is context-specific as a function of intra-individual residual correlation (see Online  
150 Methods and Table S2). In each scenario, we varied the number of individuals and contexts and  
151 the proportion of missing expression data to reflect those in GTEx [12] and the OneK1K cohort  
152 [15], two of the largest bulk and single cell RNA-Seq studies. The performance of FastGxC was  
153 systematically compared to three commonly used approaches: (1) the CxC approach, which per-  
154 forms context-by-context eQTL mapping and defines a context-specific eQTL as a variant with a  
155 significant effect in a single context, (2) MetaTissue [43], a multi-tissue eQTL mapping method  
156 that combines mixed models and meta-analysis, and defines a context-specific eQTL as a variant  
157 with a posterior probability greater than 0.9 of having an effect present in exactly one context, and  
158 (3) the linear mixed model (LMM-GxC) approach, which includes a random intercept for individ-  
159 uals to account for intra-individual residual correlation and defines a context-specific eQTL based  
160 on the significance of the genotype-by-context (GxC) interaction term (see Online Methods). To  
161 illustrate the impact of ignoring intra-individual correlation on the identification of context-specific  
162 eQTLs, we also include performance of a linear model with a GxC interaction term (LM-GxC) but  
163 no random intercept. Note that due to the large computational burden of MetaTissue, we did not  
164 obtain results for all scenarios with larger sample size (N=698).

165 We first evaluated the global type I error rates of each method for detecting an eQTL (Figure  
166 2A and S3) and for testing whether an eQTL is context-specific (Figure 2A and S4). FastGxC  
167 is well-calibrated across all tested scenarios and for both tests. LMM-GxC is generally calibrated  
168 but becomes inflated in settings with low sample size and high missing data rates. As expected,

169 both the CxC and LM-GxC approaches, which do not account for intra-individual correlation, are  
170 miscalibrated (Figure S3). As intra-individual correlation increases, LM-GxC becomes increasingly  
171 inflated for eQTL detection and increasingly conservative for testing context-specificity. The CxC  
172 approach, by contrast, remains mostly calibrated when testing for the presence of an eQTL. How-  
173 ever, depending on sample size, missing data rate, and the presence or absence of a shared eQTL,  
174 CxC becomes either increasingly conservative (Figure 2A) or anti-conservative (Figure S4) when  
175 testing for (single-)context-specificity. Finally, MetaTissue is consistently conservative in scenarios  
176 with low sample size (Figure S3) when testing for the presence of an eQTL. However, when evaluat-  
177 ing context specificity, MetaTissue becomes anticonservative or conservative, depending on whether  
178 a shared eQTL effect is present (Figure S4).

179 Next, we evaluated the global power of each method to identify an eQTL. Among the calibrated  
180 methods, FastGxC and LMM-GxC exhibit complementary strengths. FastGxC is generally more  
181 powerful when eQTL effect size heterogeneity is strong or driven by a few contexts (Figure 2B,  
182 S6-S8), as it leverages the Simes' method to combine p-values. LMM-GxC is more powerful when  
183 heterogeneity is weak but spread across many or all contexts (Figure S9-S10), due to its reliance  
184 on the likelihood ratio test (LRT). The CxC and MetaTissue approaches are less powerful than  
185 FastGxC to identify an eQTL for all scenarios with non-zero intra-individual correlation, with the  
186 power advantage of FastGxC increasing as correlation rises. The LM-GxC method is miscalibrated  
187 for eQTL detection; therefore, we do not report or discuss its power to map an eQTL.

188 For all methods, power to detect an eQTL also depends on whether variability in expression  
189 is explained by shared or context-specific effects. When the shared eQTL effect explains all ("No  
190 heterogeneity", Figure S5) or most of the expression variability ("Single-context Heterogeneity -  
191 Shared", Figure S6), power to identify an eQTL declines as intra-individual correlation increases,  
192 whereas the opposite occurs when the specific eQTL effect explains all or most variability ("Single-  
193 context Heterogeneity - No shared", Figure S6). In scenarios with intermediate shared and specific  
194 effects, power to identify an eQTL follows a U-shaped relationship with intra-individual correlation  
195 ("Extensive heterogeneity", Figure S9).

196 We next examined power to assess eQTL context specificity. For both FastGxC and LMM-  
197 GxC, power increases as intra-individual correlation increases, regardless of whether a shared eQTL

198 effect is present. Notably, FastGxC is more powerful than the CxC and MetaTissue approaches even  
199 in the single-context heterogeneity scenario without a shared effect—the scenario in which these  
200 approach are specifically used. As expected from its performance under the null, the LM-GxC  
201 method loses power to test for eQTL context specificity as intra-individual correlation increases  
202 (Figures 2B, S6–S10).

203 Then, to evaluate the ability of FastGxC to identify specific contexts driving effect size hetero-  
204 geneity, i.e. contexts most different from the shared effect, we examined the marginal type I error  
205 rate and power per context. Under the null hypothesis (“No heterogeneity”), FastGxC is calibrated  
206 for each context (FDR  $\leq 5\%$ , Figure S11). Under the alternative hypothesis, power was highest  
207 for contexts with effect sizes farthest from the shared effect and increased with intra-individual  
208 correlation (Figures 2C, S12–S14). For example, in single-context heterogeneity scenarios, FastGxC  
209 accurately identifies the context with the non-zero (“No shared” scenario) or single strongest eQTL  
210 effect (“Shared” scenario) (Figures 2C and S12).

211 In addition, we assessed FastGxC’s parameter estimation accuracy by evaluating its ability  
212 to estimate the shared (i.e.,  $\beta^{sh}$ ) and specific eQTL effect sizes (i.e.,  $\beta_c^{sp} = \beta_c - \beta^{sh}$ ) as well as the  
213 overall eQTL effect sizes in each context (i.e.,  $\beta_c = \beta^{sh} + \beta_c^{sp}$ ; Figure S16–S15). FastGxC provided  
214 unbiased estimates for the shared, specific, and overall eQTL effect sizes under conditions with no  
215 missing data or with missing data levels typical of single-cell RNA-Seq studies such as OneK1K  
216 and CLUES (approximately 5%). When the proportion of missing data was high (mean of 63%  
217 and up to 84% in some contexts), FastGxC estimates remained largely unbiased, with only slight  
218 deviations from the true effect in contexts with high missing rate.

219 Finally, we benchmarked the computational costs of FastGxC against other approaches. To  
220 obtain practical run-times, we used study parameters from GTEx, i.e., approximately 50 contexts  
221 and an average of 250 individuals per context, while varying the number of tests performed (Figure  
222 2D). When extrapolated to the entire GTEx dataset, which involves 200 million tests for 25,000  
223 genes and 3 million SNPs, we estimated that LMM-GxC and LM-GxC would require approximately  
224 30 years and 10 months, respectively, to complete. In contrast, CxC and FastGxC completed the  
225 same task in under one minute on average (based on 100 iterations). Even at a larger scale with 1,000  
226 individuals, FastGxC remained computationally efficient, completing all tests in approximately five

227 minutes, whereas LMM-GxC was estimated to take over 500 years (Figure S17). MetaTissue was  
228 not included in the runtime analysis due to its substantial computational burden, which exceeds  
229 that of LMM-GxC.

230 **Context-specificity of eQTLs is widespread across tissues and PBMC cell types.** To  
231 evaluate performance in bulk tissue, we applied FastGxC to multi-tissue RNA-Seq data from the  
232 GTEx consortium (N = 698 individuals, 49 tissues) [12], identifying cis-eQTLs and assessing their  
233 tissue specificity. To assess performance in single-cell data, we applied FastGxC to peripheral blood  
234 mononuclear cells (PBMCs) from the CLUES [14] and OneK1K [15] cohorts (N = 237 and N =  
235 981 individuals, respectively, across 8 cell types), and performed meta-analysis to map cis-eQTLs  
236 and evaluate their cell type specificity (Online Methods). Before quantifying cis-regulation, we  
237 confirmed that FastGxC reduces background noise, as the top principal components (PCs) of the  
238 decomposed expression data showed minimal correlation with technical and biological covariates  
239 compared to the original GTEx data (Figure S1).

240 We then assessed the extent of cis regulation and how context-specific these effects are across  
241 tissues and cell types (Figure 3). We identified a total of 24,196 eGenes across tissues (70.21% of  
242 tested genes) and 4,564 eGenes across cell types (29.05% of tested genes), defined as genes with  
243 at least one eQTL in any context (hierarchical FDR (hFDR)  $\leq 5\%$ , Table S5). The majority of  
244 FastGxC eGenes (86.5% and 82.7% across tissues and cell types) had at least one shared eQTL  
245 (Figure 3A), aligning with previous observations of widespread cis regulation and eQTL sharing  
246 [12, 34]. Despite extensive sharing, effect sizes varied substantially between contexts, with 72.1% of  
247 tissue eGenes and 63.9% of PBMC cell-type eGenes harboring at least one context-specific eQTL  
248 (Figure 3A). Notably, most of these context-specific eQTLs overlapped with shared eQTL loci  
249 (81.3% and 73.1% across tissues and cell types), suggesting that context-specificity often arises  
250 from effect size heterogeneity rather than the presence of an eQTL in a single context (Figure 3A).  
251 Representative examples illustrating shared-only and shared-plus-specific effects are discussed in  
252 the supplement (Figure S19).

253 We next aimed to determine how many and which context(s) drive the effect size heterogeneity  
254 for eGenes with context-specific eQTLs (Figure 3B-C and S3). In both bulk and single-cell data, we

255 observed that the majority of specific eQTLs are identified in only a few contexts (Figure 3C). In  
256 tissues, much of the heterogeneity is driven by testis (6,124 eGenes), followed by whole blood (5,219  
257 eGenes), consistent with findings from studies mapping eQTLs specific to a single tissue. [12]. Testis,  
258 which is biologically distinct from other GTEx tissues, also contributes the largest proportion (16%)  
259 of single-context-specific eQTLs—i.e., eQTLs unique to a single tissue—highlighting FastGxC’s  
260 ability to detect biologically meaningful context-specific regulation (Figure 3D). For PBMC cell  
261 types, CD4 cells (1,907 eGenes) and classical monocytes (980 eGenes) account for the majority of  
262 the heterogeneity and also contain the highest number of eQTLs unique to a single cell type. Both  
263 the number of specific eGenes and single-context specific eGenes per context are strongly correlated  
264 to the number of samples per tissue and the number of cells per cell type (Figure S18A), indicating  
265 that we may not yet have reached saturation in identifying these context-specific regulatory effects.

266 We next compared the eGenes identified by FastGxC to those identified by the CxC ap-  
267 proach. Consistent with our simulation results, FastGxC identified substantially more eGenes than  
268 CxC, detecting an additional 2,159 eGenes in bulk tissues and 679 eGenes in PBMC cell types  
269 (Figure S18B). Broadly, most (96.6% in tissues and 62.8% in PBMCs) FastGxC shared eQTLs  
270 overlapped with eQTLs detected in multiple contexts by CxC (Figure 4A). Importantly, FastGxC  
271 single-context-specific eQTLs mapped almost exclusively to single-context-specific eQTLs detected  
272 by CxC, demonstrating strong concordance in these cases. However, a substantial fraction (48.1%  
273 in tissues and 43.1% in PBMC cell types) of CxC single-context-specific eQTLs corresponded to  
274 FastGxC shared-only eQTLs. This discrepancy reflects the false positive specific effects that the  
275 CxC approach tends to identify — an issue we also observed in simulation results (Figure S4). More-  
276 over, the number of context-specific eQTLs detected by CxC showed a stronger correlation with  
277 sample size than FastGxC (Figure S18A), further highlighting its sensitivity to power differences  
278 across contexts. These results underscore the limitations of CxC approaches that define context-  
279 specificity solely by the presence of significant eQTLs in isolated contexts, rather than accounting  
280 for heterogeneity in effect sizes.

281 Finally, we show that context-specific eQTL effect sizes are correlated within groups of bi-  
282 ologically related tissues and cell types. For example, we see that context-specific eQTL effects  
283 are correlated among 13 brain, two heart (left ventricular and atrial appendage), two artery (tibial

284 and aorta), two esophagus (muscularis and gastro-esophageal junction), three adipose (visceral,  
285 subcutaneous, and breast), and two intestine tissues (Figure 4B - right triangle). In addition,  
286 context-specific eQTL effects are correlated most across CD4 and CD8 cells, NK cells, and B cells,  
287 between plasmacytoid and conventional dendritic cells, as well as between classical and non-classical  
288 monocytes. Furthermore, while FastGxC context-specific eQTL effect sizes show little to no corre-  
289 lation outside groups of biologically related tissues and cell types, CxC effect sizes show widespread  
290 correlation across all tissues and cell types regardless of biological relationships (Figure 4B - left  
291 triangle). This again demonstrates that FastGxC is able to disentangle tissue and cell type specific  
292 effects from shared effects.

293 **Context-specific eQTLs are enriched in functional genomic features from their matched**  
294 **context.** To investigate functional differences between shared and context-specific eQTL variants,  
295 we performed enrichment analysis of regulatory genomic elements, comparing variants with only  
296 shared or only context-specific effects to MAF-matched non-eQTL variants (Figure 5A, right panel).  
297 In bulk tissues, variants with context-specific effects were enriched within enhancers (Odds Ratio  
298  $[OR] = 1.06, p = 1.16 \times 10^{-5}$ , FDR  $\leq 5\%$ ), while those with shared effects were depleted ( $OR = 0.98$ ,  
299  $p = 2.87 \times 10^{-2}$ ). Both sets of variants were enriched within promoters but the enrichment was  
300 stronger for variants with shared effects ( $OR = 1.14, p = 1.39 \times 10^{-37}$ ) compared to those with  
301 specific effects ( $OR = 1.04, p = 3.14 \times 10^{-2}$ ) only. In single cell PBMC cell types, we see a similar  
302 trend for enhancers ( $OR_{shared} = 0.98$  and  $OR_{specific} = 1.02$ ) but the enrichment is not significant  
303 after multiple testing adjustment, likely because the number of variants with only shared or specific  
304 effects is much smaller for single cell than bulk data. In addition, variants with shared effects  
305 only were enriched within promoters ( $OR = 1.10, p = 5.34 \times 10^{-13}$ ), while those with specific  
306 effects were depleted ( $OR = 0.88, p = 8.26 \times 10^{-6}$ ). These findings are consistent with previous  
307 observations that variants with context-specific effects are more enriched in genomic elements that  
308 confer context specificity to gene expression, such as enhancers, while variants with shared effects  
309 are more common within promoters [18, 44].

310 To understand how variants with eQTL effects mapped by the CxC approach differ func-  
311 tionally from those identified by FastGxC, we performed another enrichment analysis for genomic

312 elements using sets of variants that are only discovered by CxC or FastGxC (Figure 5A right panel).  
313 Compared to CxC-only variants, FastGxC-only variants are enriched ( $FDR \leq 5\%$ ) in more genomic  
314 features (50% versus 12.5% of annotations in tissues and 87.5% versus 37.5% in PBMCs) and show  
315 stronger enrichment in key genomic elements, such as CTCF binding sites ( $OR_{FastGxC} = 1.08$  and  
316  $OR_{CxC} = 1.04$  in tissues and  $OR_{FastGxC} = 1.07$  and  $OR_{CxC} = 1.03$  in PBMCs). Additionally, in  
317 tissues, FastGxC-only variants are significantly enriched in enhancers ( $OR = 1.05, p = 2.1 \times 10^{-3}$ ),  
318 while CxC-only variants are not ( $OR = 1.02, p = 1.8 \times 10^{-1}$ ). In PBMCs, FastGxC-only variants  
319 are depleted in enhancers but are enriched in every other genomic feature that we tested.

320 Chromatin is strongly context-specific [45] and therefore provides a natural framework for  
321 validating FastGxC-mapped context-specific eQTLs and quantifying the functional differences be-  
322 tween FastGxC and CxC-mapped eQTLs. To this end, we tested for enrichment of variants with  
323 FastGxC or CxC single-context-specific eQTL effects in regions of open chromatin from matching  
324 tissues and cell types. Among bulk tissues, FastGxC variants were more often enriched in open  
325 chromatin from the corresponding tissues compared to CxC variants, with enrichment observed in  
326 54% (29/54) versus 30% (16/54) of cases (One-sided McNemar test,  $p = 1.95 \times 10^{-3}$ ; Figure 5B).  
327 Additionally, we observed widespread enrichment in open chromatin for both FastGxC and CxC  
328 variants in tissues with broadly distributed cell types, such as whole blood [46, 47]. In PBMCs, four  
329 out of six (66.6%) cell types with matching chromatin data demonstrated significant enrichment  
330 in open chromatin regions from corresponding cell types versus 50% of cell types for CxC eQTLs  
331 (One-sided McNemar test,  $p = 1$ ). CD4 and CD8 cells lacked significant enrichment ( $FDR \leq 5\%$ )  
332 within the broader T cell group, likely due to the aggregation of more granular subtypes, reducing  
333 specificity (see Methods) but the enrichment trend is similar ( $OR_{CD4} = 1.03$  and  $OR_{CD8} = 1.34$ ).

334 Together, these results highlight the functional relevance of FastGxC context-specific eQTLs,  
335 showing greater enrichment in functional genomic elements and improved capture of context-specific  
336 chromatin accessibility in matched contexts compared to CxC eQTLs. Additionally, context-specific  
337 eQTLs identified exclusively by FastGxC are more likely to reside in functional regions.

338 **Context-specific eQTLs identify putatively causal contexts and genes of complex traits.**  
339 Mapping eQTLs is crucial for identifying the regulatory targets and context of action of disease-

340 associated non-coding variation. To evaluate whether FastGxC eQTLs improve our understanding  
341 of the context mediating complex disease risk, we analyzed trait-associated variants from 539 traits  
342 in the NHGRI-EBI GWAS catalog [48]. Specifically, we tested for enrichment of variants with  
343 specific and shared eQTL effects identified by FastGxC in trait-associated variant sets, comparing  
344 them to an equal-sized set of MAF-matched non-eQTL variants (Table S5). Following the GTEx  
345 consortium protocol, we used expert curation to assign the most relevant tissues for each trait (Table  
346 S5) [12] and assessed precision and recall rates to identify the tissue labeled as relevant for each  
347 trait. These results were compared with those obtained from CxC eQTLs in individual contexts.  
348 PBMC cell types were excluded from this analysis due to the uncertainty regarding the exact cell  
349 type relevant for each trait.

350 At the same recall rate, FastGxC eQTLs achieved a three-fold increase in precision for identi-  
351 fying disease-relevant tissues and a two-fold improvement in their ranking compared to CxC eQTLs  
352 (Figure 6A). While CxC eQTLs typically prioritized a median of 10 out of 49 tissues per trait,  
353 likely due to widespread tissue-sharing (Figure 4B), FastGxC prioritized a median of two tissues.  
354 This suggests that modeling the extensive sharing of eQTL effects across tissues can better localize  
355 GWAS associations to a smaller, more relevant subset of tissues.

356 Overall, FastGxC enrichment patterns aligned well with known trait-tissue associations (Fig-  
357 ure 6B,  $\text{FDR} \leq 5\%$ ). In cancer traits, where the relevant tissue is typically well-defined, FastGxC  
358 demonstrated superior tissue localization compared to CxC. For instance, in breast carcinoma,  
359 FastGxC showed the strongest enrichment in breast mammary tissue ( $OR = 5.0, p = 3.2 \times 10^{-4}$ ),  
360 while CxC prioritized EBV-transformed lymphocytes, with breast mammary tissue ranking 25th  
361 ( $OR = 2.24, p = 7.5 \times 10^{-4}$ ). In lung adenocarcinoma, CxC identified significant associations in  
362 22 tissues, many unrelated to lung physiology (lung  $OR = 2.83$ , ranked 18th,  $p = 1.6 \times 10^{-3}$ ),  
363 whereas FastGxC found associations only in lung ( $OR = 5.67, p = 2.60 \times 10^{-3}$ ) and nerve tibial  
364 ( $OR = 20, p = 2.1 \times 10^{-5}$ ). For traits not specific to a single tissue, such as the “any cancers” trait,  
365 FastGxC showed the strongest enrichment for shared eQTLs, consistent with processes common  
366 across tissues. This improved tissue resolution was also evident in non-cancer traits. For example,  
367 in coronary artery disease, FastGxC identified significant associations in 17 tissues, compared to 43  
368 for CxC, with the top tissues being cardiovascular-relevant, such as coronary ( $OR = 13.0$ , ranked

369 1st) and aortic ( $OR = 2.96$ , ranked 2nd) artery, heart left ventricle ( $OR = 2.82$ , ranked 5th), and  
370 atrial appendage ( $OR = 2.37$ , ranked 8th).

371 To evaluate the ability of FastGxC eQTLs to identify the regulatory targets of trait-associated  
372 variants, we performed a colocalization analysis integrating GWAS summary statistics for 63 com-  
373 plex traits and diseases with FastGxC shared and specific eQTLs in bulk tissues and single-cell  
374 PBMC types (Figure 6C and Table S6). We compared these results to colocalizations based on  
375 CxC eQTLs mapped separately in each tissue and PBMC cell type. Across all traits and methods,  
376 we prioritized candidate causal genes for 5,726 (47.12% of tested) GWAS loci at a colocalization  
377 posterior probability (CLPP) threshold of 50%. The majority of the colocalizations (83.56% in  
378 tissues and 61.75% in PBMC cell types) were identified by both methods, while 6.40% and 20.18%  
379 were unique to FastGxC in tissues and PBMC cell types, respectively. This represents a 6.84%  
380 and 25.28% increase in significant colocalizations for tissues and PBMCs, respectively (Figure 6C),  
381 with the percentage increase remaining relatively consistent across CLPP thresholds for tissues and  
382 reaching up to 50% for PBMCs (Figure S20).

383 Previous studies suggest that context-specific eQTLs are more enriched for disease associations  
384 than shared eQTLs (12, 14). To test this hypothesis, we compared the colocalization rates of  
385 FastGxC shared and specific eQTLs. In tissues, most colocalizations (54.25%) involved eQTLs  
386 with both shared and context-specific effects, while 33.80% were specific-only eQTLs. In PBMCs,  
387 colocalizations were highest for shared-only eQTLs (40.93%), followed by those with both shared and  
388 specific effects (32.62%, Figure 6C). However, after normalizing by the number of shared and specific  
389 eQTLs tested for colocalization, specific eQTLs showed higher colocalization rates than shared  
390 eQTLs in both tissues (41.52% vs. 32.19%, One-sided Binomial proportion test  $p = 1.25 \times 10^{-91}$ )  
391 and PBMCs (29.78% vs. 25.93%  $p = 0.108$ ) (Figure 6C). This represents a 1.2-fold enrichment  
392 in the ability of specific eQTLs to identify candidate causal genes for trait-associated variants,  
393 reinforcing their disease relevance.

394 Taken together, we demonstrate that FastGxC-specific eQTLs enhance the resolution of  
395 context-trait associations, increase the number of candidate causal genes for human traits, and  
396 are more disease relevant than shared eQTLs.

### 397 3 Discussion

398 We developed FastGxC, a novel statistical method for efficiently and powerfully mapping context-  
399 specific eQTLs by leveraging the correlation structure of functional genomic studies with repeated  
400 sampling. Through simulations, we demonstrated that FastGxC is well-calibrated for both iden-  
401 tifying eQTLs and assessing their context specificity. Furthermore, FastGxC provides unbiased  
402 estimates of overall eQTL effect sizes in each context, with only slight bias in cases of extensive  
403 missing data (over 63% of data missing). FastGxC matches the power of LMM-GxC—the only other  
404 properly calibrated method for context-specific eQTL mapping—while being orders of magnitude  
405 faster.

406 We applied FastGxC to bulk multi-tissue and single-cell RNA-seq data sets and identified  
407 17,447 tissue-specific and 2,920 cell-type-specific eGenes. The majority of context-specific effects  
408 appeared in loci that exhibited context-shared effects, highlighting the importance of defining  
409 context-specificity by effect size heterogeneity rather than the presence or absence of significant  
410 eQTL effects in each context. In addition, we found that context-specific eQTLs are shared mostly  
411 between groups of biologically related contexts and are more frequently enriched in genomic ele-  
412 ments that confer context specificity to gene expression, e.g., enhancers and context-specific regions  
413 of open chromatin, providing further evidence of their validity. Finally, we found that context-  
414 specific eQTLs provide increased precision for identifying disease-relevant contexts compared to  
415 CxC eQTLs, and FastGxC specific eQTLs provided a 1.2 fold increase over shared eQTLs to iden-  
416 tify putative causal genes that drive human traits, confirming their utility in understanding the  
417 regulatory mechanisms underlying complex human diseases.

418 Despite its advantages, FastGxC has certain limitations that warrant consideration. For single-  
419 cell RNA-seq data, FastGxC operates on pseudo-bulked data, aggregating expression profiles across  
420 cells within the same context. While this approach may lead to power loss in cases of substantial  
421 cell-to-cell heterogeneity within cell types, prior studies suggest that pseudo-bulk methods perform  
422 comparably to single-cell approaches [31, 49]. Additionally, FastGxC relies on predefined contexts,  
423 which can be challenging in single-cell data due to the lack of a unified framework for defining  
424 and classifying cell types [50]. Finally, while FastGxC’s marginal tests are well-calibrated, their

425 utility diminishes in cases of extensive heterogeneity, where many contexts contribute to effect  
426 size variation (Figure S14). In addition, the context driving heterogeneity can be one without a  
427 detected eQTL—e.g., if all but one context have a significant eQTL, the remaining context will  
428 exhibit the largest (absolute) context-specific effect size (Figure S14). This highlights the nuances  
429 of interpreting context specificity in these scenarios. Nevertheless, in real-world data, FastGxC  
430 performs well, as evidenced by the enrichment of its context-specific eQTLs in functional genomic  
431 annotations and disease associations.

432 Additional extensions of FastGxC have the potential to further improve the power and scal-  
433 ability of the method, but we leave these directions to future work. The current implementation  
434 models a single shared component across all contexts, which performs well in many datasets. How-  
435 ever, this formulation does not identify which specific contexts contribute to the shared signal and  
436 may fail to capture finer subgroup structures, such as sets of closely related tissues (e.g., brain  
437 regions in GTEx). We have previously shown that incorporating hierarchical decompositions can  
438 refine estimates of context-group-specific and context-specific eQTL effects [51]. Moreover, Fast-  
439 GxC defines specificity as deviation from the average effect across contexts, but some studies, such  
440 as time-course or environmental perturbation experiments, may require comparisons against a base-  
441 line context. Adjusting the decomposition step to accommodate these cases is straightforward and  
442 could expand FastGxC’s applicability. Furthermore, FastGxC assumes normally distributed ex-  
443 pression residuals after rank-based inverse normal transformation. Extending FastGxC to handle  
444 non-normal phenotypes using generalized linear models [31, 33, 52] is straightforward but could be  
445 computationally costly. Similarly, FastGxC can be extended to capture non-linear genetic effects  
446 [30] but at a considerable computational cost and likely limited yield at current single cell sample  
447 sizes. Further improvements could come from integrating methods that model shared effect patterns  
448 across contexts [34] and incorporating fine-mapping approaches like [53] to refine candidate causal  
449 variants within significant loci, both of which are compatible with FastGxC.

450 In conclusion, we show that accounting for the intra-individual correlation and extensive  
451 sharing of eQTLs across contexts reveals context-specific eQTLs that can aid downstream interpre-  
452 tation of disease-associated variants. Furthermore, we highlight the importance of defining context  
453 specificity based on effect size heterogeneity, rather than relying on heuristic definitions and miscal-

454 vibrated tests. We anticipate that applying FastGxC to the growing number of multi-context bulk  
455 and single-cell RNA-Seq studies will significantly expand our understanding of the context-specific  
456 gene regulatory mechanisms underlying complex human diseases.

457 **Acknowledgements** B.B. is supported by NIH grants U01HG012079, R01MH125252, R01DK132775,  
458 and R01DK137889. M.T. is supported by EMBO Fellowship ALTF 266-2023. L.K. is supported by  
459 NIH T32 781460-VA-32187-05. I.C is supported by a Ikerbasque Research Fellowship, funded by the  
460 EU (H2020-MSCA-COFUND-2020-101034228-WOLFRAM2), and grant PID2023-148986OB-I00  
461 funded by MCIU/AEI/FEDER-EU. N.Z. is supported by NIH grants R01HG006399, R01CA227237,  
462 R01CA227-466, R01ES029929, R01MH122688, U01HG009080, R01HG011345, R35GM133531, R01HL155024,  
463 R01MH125252, DoD grant W81XWH-16-2-0018, and the Chan Zuckerberg Science Initiative. C.J.Y.  
464 is supported by the NIH grants R01AR071522, R01AI136972, R01HG011239, and the Chan Zuckerberg  
465 Science Initiative, and is an investigator at the Chan Zuckerberg Biohub and a member of the  
466 Parker Institute for Cancer Immunotherapy. J.W.K. is supported by the NIH grants P30 DK116074  
467 (to the Stanford Diabetes Research Center), R01 DK116750, R01 DK120565, R01 DK106236, R01  
468 DK139112. The GTEx Project was supported by the Common Fund of the Office of the Director  
469 of the National Institutes of Health, and by NCI, NHGRI, NHLBI, NIDA, NIMH, and NINDS.

470 **Author contributions** B.B. conceived of the project and developed the statistical methods.  
471 A.L., C.L., and B.B. implemented the comparisons with simulated data. A.L., L.K., B.B., M.T.,  
472 A.R., and M.G.G. performed the analyses of the GTEx, OneK1K, and CLUES data and additional  
473 analyses. A.R. and L.K. performed the colocalization analysis. B.B., A.L., and L.K. implemented  
474 the software. A.L., L.K., and B.B. wrote the manuscript, with significant input from N.Z., C.J.Y.,  
475 A.D., M.G.G., and M.T. A.L., L.K., and B.B. prepared the online code and data resources. All  
476 authors read and approved the manuscript.

477 **Data and code availability** The FastGxC software is available as an R package at <https://github.com/BalliuLab/FastGxC>. All data and code to reproduce the manuscript Figures are avail-  
478 able at [https://github.com/BalliuLab/FastGxC\\_Manuscript](https://github.com/BalliuLab/FastGxC_Manuscript). The map of shared and context-  
479 specific eGenes, as well as GWAS enrichment and colocalization results for all GTEx tissues and all

481 PBMCs, are available as supplementary tables [S4](#) - [S6](#). Data used to replicate GTEx and PBMC  
482 eQTLs are available via the GTEx portal and GEO (see Online Methods).

483 **Declaration of interests** C.J.Y. is a Scientific Advisory Board member for and hold equity in  
484 Related Sciences and ImmunAI, a consultant for and hold equity in Maze Therapeutics, and a  
485 consultant for TReX Bio. C.J.Y. has received research support from Chan Zuckerberg Initiative,  
486 Chan Zuckerberg Biohub, and Genentech.

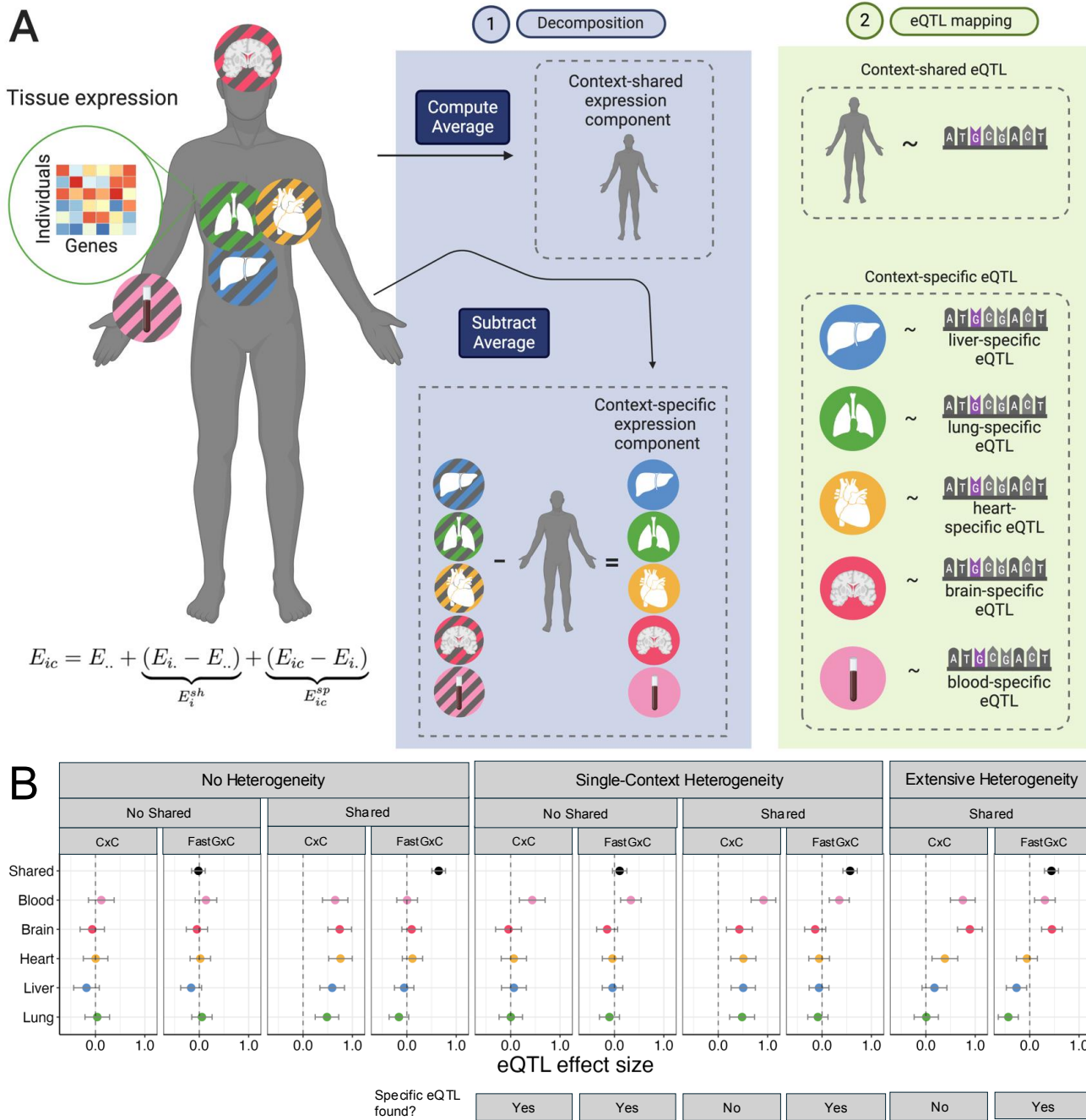


**Figure 1. Overview of the FastGxC method and toy examples of eQTLs. A.** FastGxC decomposes gene expression for each individual into a context-shared component and context-specific components (Step 1). It then estimates both the shared eQTL effect across contexts and the context-specific eQTL effects within each context by regressing genotypes on these components (Step 2). **B.** Toy examples of eQTLs. Y axis and color represent the context and x axis lists the eQTL effect. The first example represents a scenario with no eQTLs in any tissue and, thus, no shared or specific eQTLs. The second example represents a scenario with equal eQTL effects across all tissues, corresponding to a scenario with a shared eQTL but no specific eQTLs. The third, fourth, and fifth examples correspond to a scenario with an eQTL in which a single context (e.g., blood) or multiple contexts drive the effect size heterogeneity.

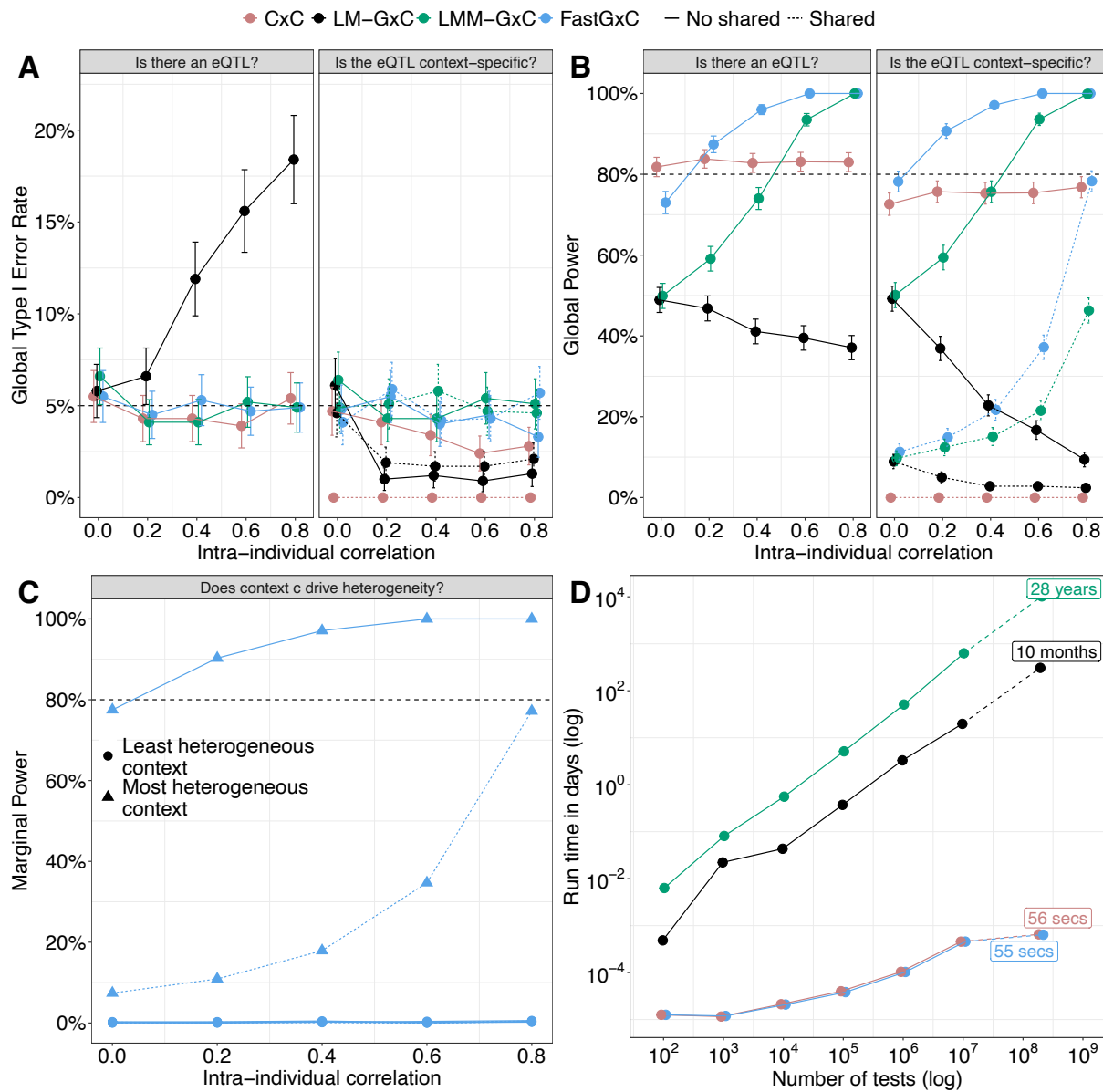


**Figure 2. FastGxC outperforms existing methods in simulated data.** **A-B.** Global Type I error rate (A) and global and marginal power (B and C) for detecting an eQTL (A and B - left panel), testing for context-specificity of its effect (A and B - right panel), and identify which context drives the heterogeneity (C) under the no heterogeneity (A) and single-context heterogeneity (B, C) scenarios (Figure 1B) across different levels of intra-individual correlation (rows). For effect sizes in each scenario, see Table S2. For power under the two-context and extensive heterogeneity scenarios, see Figures S8 - S10. For marginal Type I error rates and marginal power under the two-context and extensive heterogeneity scenarios see Figures S11 - S14. Figure panels A-C show results from simulations with 698 individuals and 49 contexts and GTEX missing data patterns (63%). For results without or less missing data, lower sample size, and fewer contexts see Figures S3 - S14. **D.** Run time for all methods for varying number of tests performed in a sample size of 250 individuals (average sample size across tissues in GTEX). See Figure S17 for sample size of 1,000 individuals. Last points reflect projected run time for entire GTEX data-set - 50 contexts, 25K x 3M tests, and 250 samples per context. Analyses were run on 8 cores on a 2.70 GHz Intel Xeon Gold Processor on the UCLA Hoffman2 Computing Cluster.

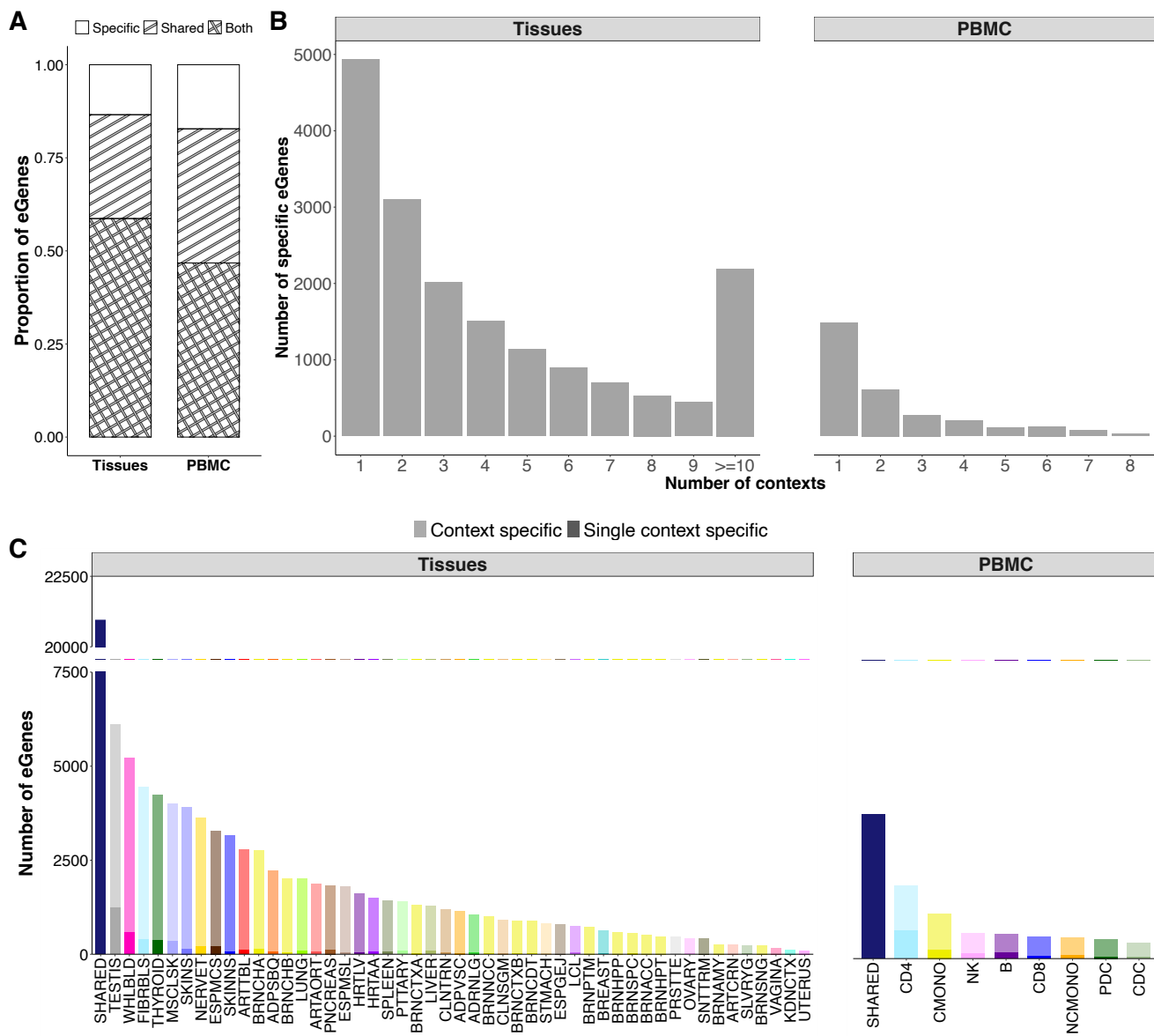


**Figure 3. Context-specific eQTL mapping in bulk tissues and single-cell PBMC cell types.** **A.** Percent of eGenes with shared-only ("Shared"), specific-only ("Specific"), and both specific and shared ("Both") eQTLs across all tissues (left) and PBMC cell types (right). **B.** Number of contexts that drive the effect size heterogeneity for eGenes with context-specific eQTLs across tissues (left) and PBMC cell types (right). **C.** Number of eGenes with shared and context-specific eQTLs per context. For eGenes with context-specific eQTLs, opacity of color indicates the number of eGenes with specific eQTLs shared with other contexts (lightest opacity) or specific eQTLs unique to that context (darkest opacity). Tissue and cell type abbreviations are explained in Table S3.

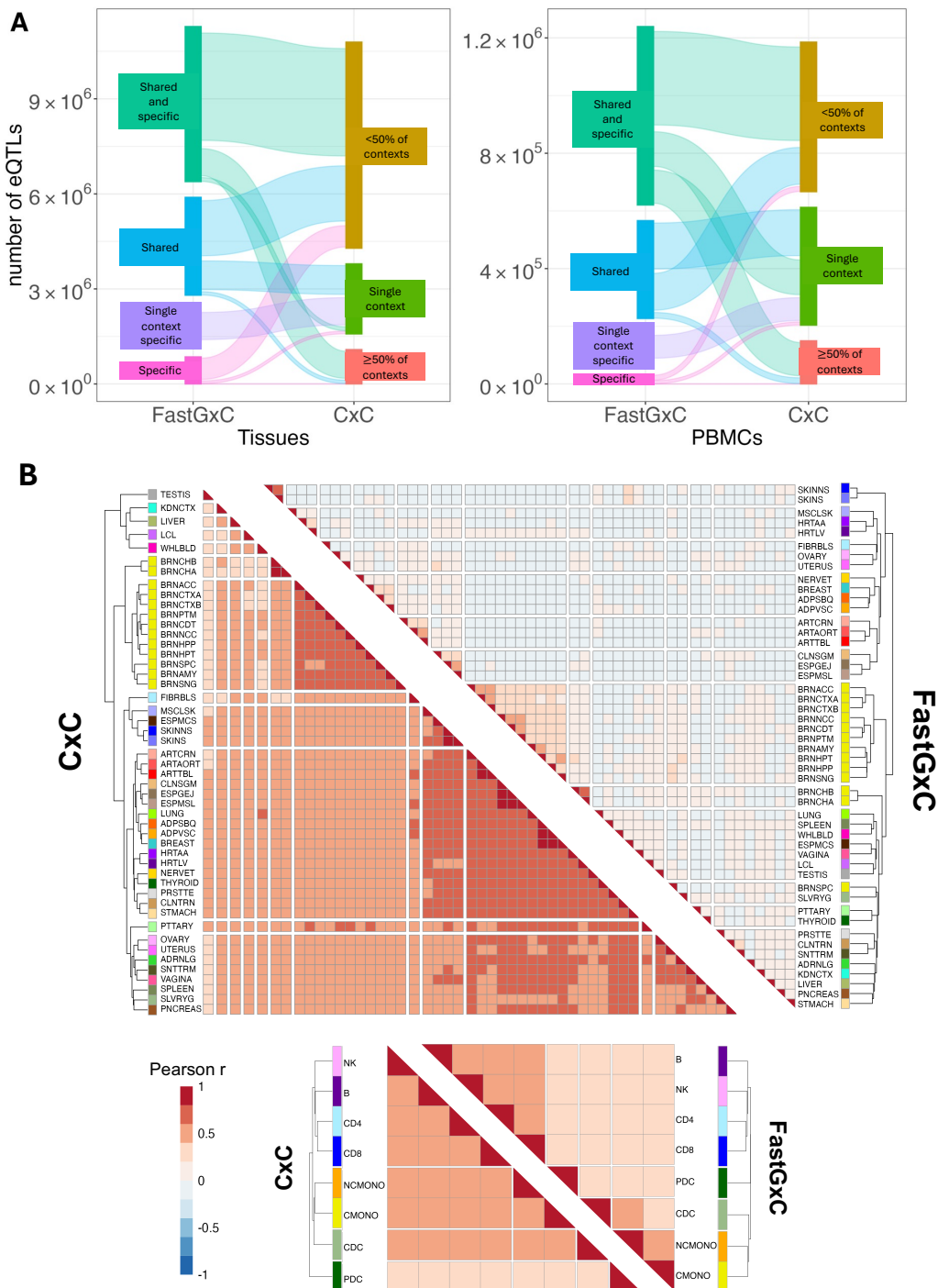
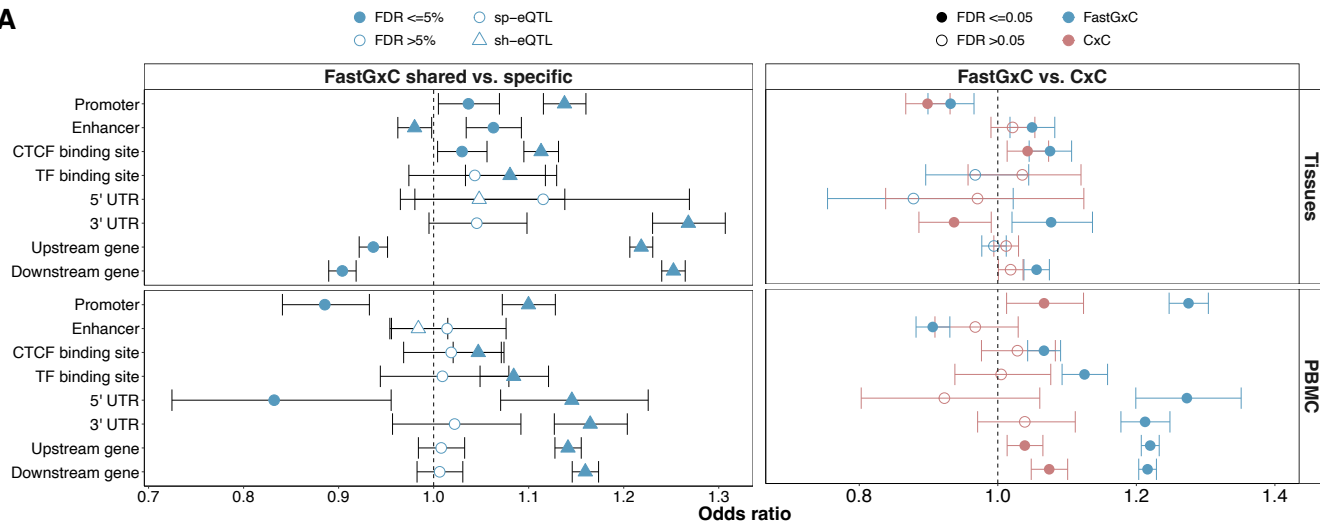


**Figure 4. FastGxC specific eQTLs are concordant with CxC, and have strong effect size correlations among biologically related contexts.** **A.** Sankey diagrams showing how eQTLs identified by FastGxC match to eQTLs identified by CxC in both tissues (left) and PBMCs (right). Node colors represent categories of eQTLs classified by CxC and FastGxC. FastGxC categories include single-context-specific eQTLs (single context specific), eQTLs that are shared or specific only (Shared, Specific), and eQTLs that are both shared and specific (Shared and specific). CxC categories include eQTLs that are found only in a single context (single context), eQTLs found in more than 1 context but <50% of contexts (<50% of contexts), and eQTLs found in  $\geq 50\%$  of contexts ( $\geq 50\%$  of contexts). **B.** Heatmap with Pearson's correlation of CxC eQTL effect sizes (left) and FastGxC context-specific eQTL effect sizes (right) across tissues (top) and PBMC cell types (bottom). Tissue and cell type abbreviations are explained in Table S3.

**A**



**B**

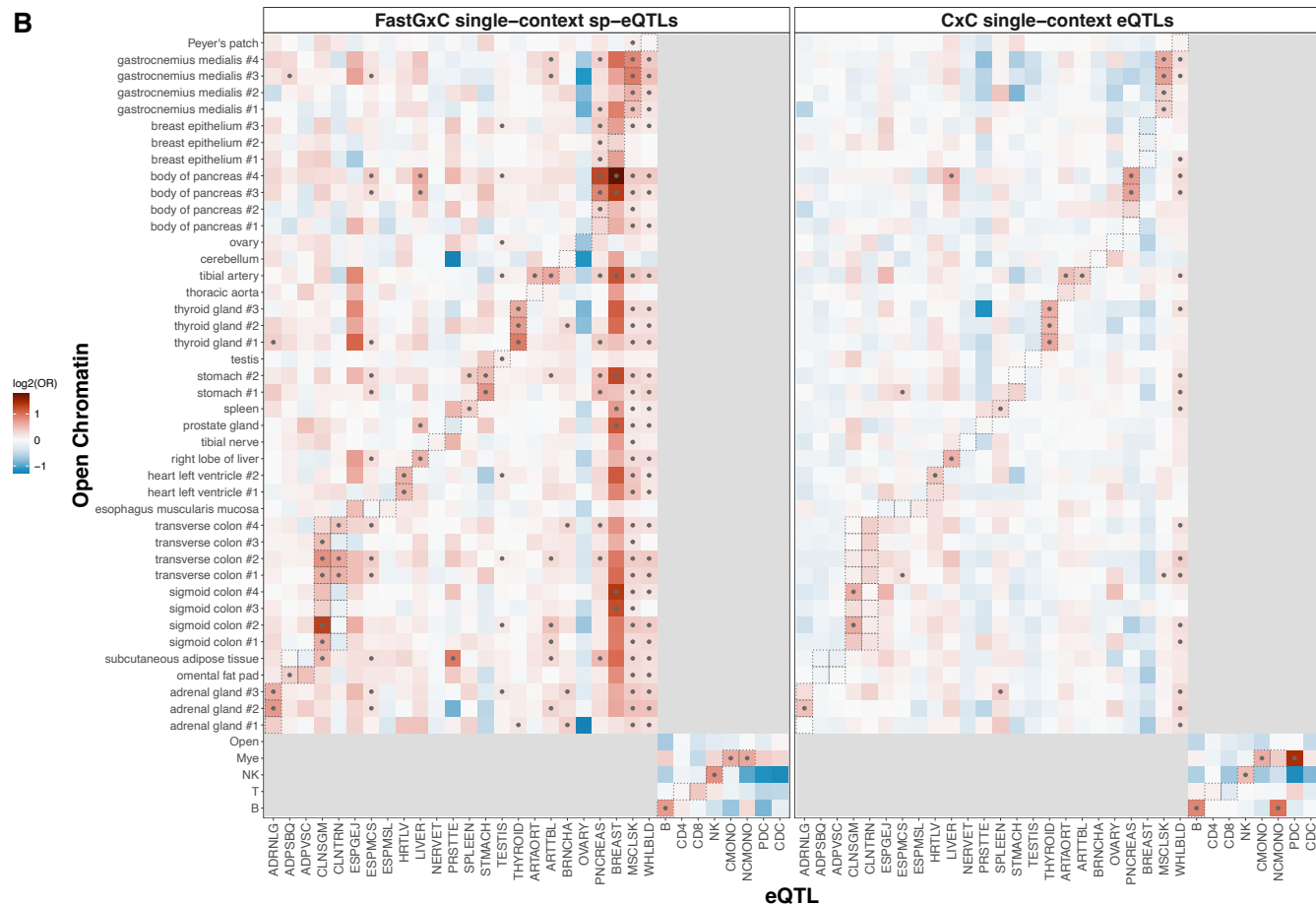


**Figure 5. Context-specific eQTL variants are enriched in functional genomic features from their respective contexts.** **A.** Enrichment of variants with FastGxC shared or context-specific effects only (left) and variants discovered by FastGxC or CxC only (right) across tissues (top) and PBMCs cell types (bottom) in genomic elements with known regulatory effects. Shape indicates different sets of variants. Color indicates different methods. Shape fill indicates significance of enrichment at  $FDR \leq 5\%$ . **B.** Enrichment of variants with FastGxC context-specific (left) or CxC (right) eQTL effects that are unique to a single context in regions of open chromatin across multiple tissues and cell types. Tissue and PBMC cell type open chromatin regions were obtained from ENCODE and Calderon et al. [21], respectively. Boxes indicate manual matching between chromatin and expression context. Color indicates strength of enrichment/depletion in  $\log_2$  scale. Dot indicates significant enrichment at  $FDR \leq 5\%$ .

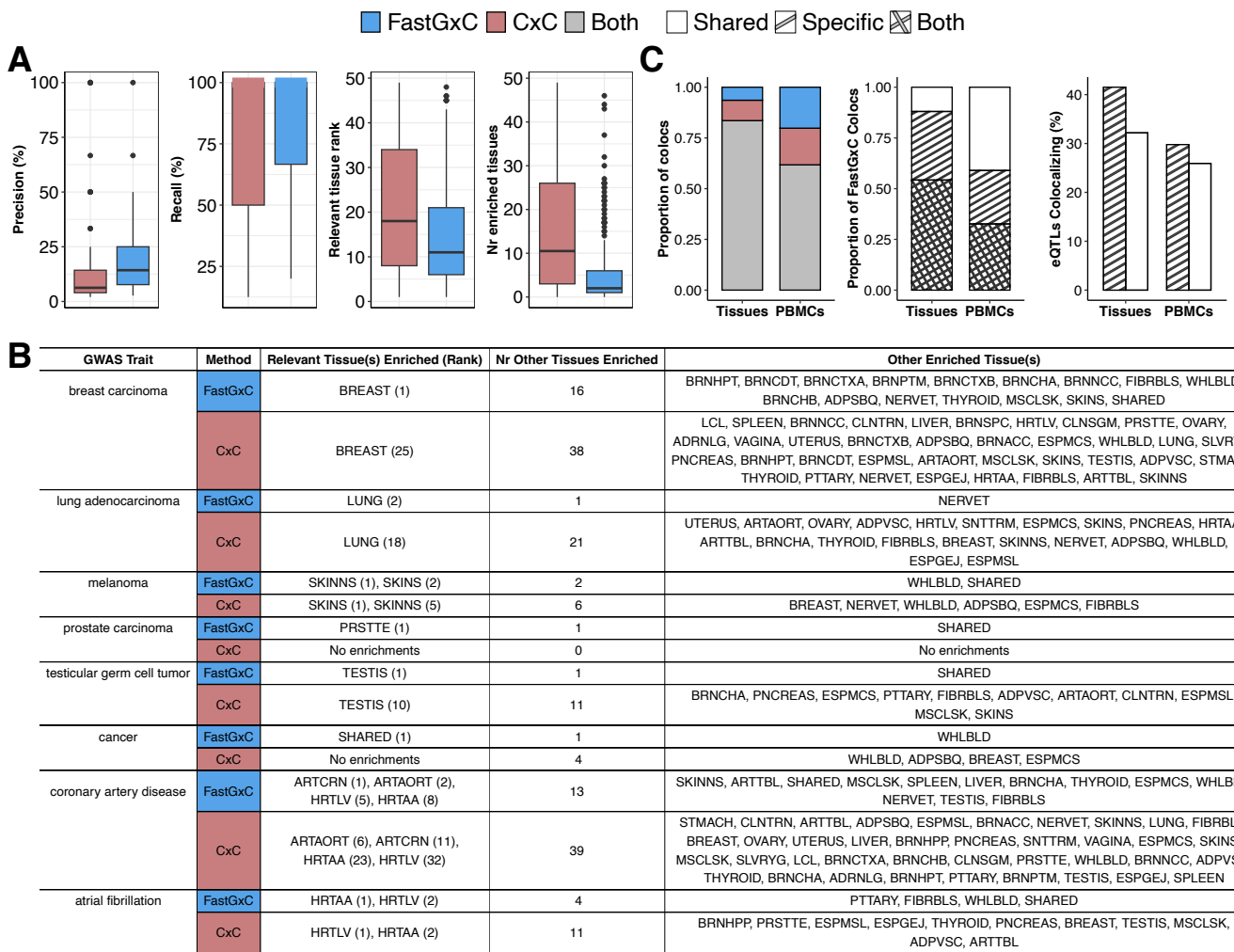


**Figure 6. FastGxC identifies context-relevant mechanisms and increases colocalizations of complex traits.** **A.** Accuracy of FastGxC and CxC eQTLs to prioritize the most relevant tissue(s) across 539 complex traits with a strong prior indication for the likely relevant tissue(s). Number of enriched tissues for each method was computed only for traits that had at least one significant enrichment in either method. **B.** Tissues prioritized by FastGxC and CxC eQTLs as well as the rank of the known relevant tissues for specific complex traits. **C.** Colocalization of FastGxC and CxC eQTLs with GWAS summary statistics across 63 human traits. **Left:** Proportion of colocalizations found uniquely by FastGxC or CxC and by both methods. **Middle:** Proportion of FastGxC identified colocalizations that are shared-eQTLs only, specific-eQTLs only, or both. **Right:** Percentage of FastGxC shared and specific eQTLs that co-localized over the total number of shared and specific eQTLs tested for colocalization for tissues and PBMCs.

## 487 Online Methods

488 **Overview of FastGxC method** Let  $E_{ic}$  be the observed expression of a gene for individual  
 489  $i$  ( $i = 1, \dots, I$ ) in context  $c$  ( $c = 1, \dots, C$ ). FastGxC first decomposes  $E_{ic}$  into an offset term, a  
 490 context-shared component, and a context-specific component [54], i.e.

491

$$E_{ic} = E_{..} + \underbrace{(E_{i..} - E_{..})}_{E_i^{sh}} + \underbrace{(E_{ic} - E_{i..})}_{E_{ic}^{sp}} \quad (1)$$

492 where  $E_{..} = \left( \sum_{i=1}^I \sum_{c=1}^C E_{ic} \right) / (I \times C)$  is the average expression of the gene, computed over  
 493 all  $I$  individuals and all  $C$  contexts, and  $E_{i..} = \left( \sum_{c=1}^C E_{ic} \right) / C$  is the average expression of the gene  
 494 for individual  $i$ , computed over all contexts. In (1),  $E_{..}$  is a term that is constant across individuals  
 495 and contexts for each gene,  $E_i^{sh}$  is the context-shared expression component for individual  $i$  and is  
 496 constant across contexts for each gene and individual, and  $E_{ic}^{sp}$  is the context- $c$ -specific expression  
 497 component for individual  $i$ .

498 Next, FastGxC estimates one shared and  $C$  context-specific cis genetic effects by regressing  
 499 the genotypes on each component using ultra-fast implementations of fixed-effect linear regression  
 500 models [38], i.e.,

501

$$E_i^{sh} = \alpha^{sh} + \beta^{sh} G_i + \varepsilon_i^{sh},$$

502

$$E_{i1}^{sp} = \alpha_1^{sp} + \beta_1^{sp} G_i + \varepsilon_{i1}^{sp},$$

503

$$\vdots$$

504

$$E_{iC}^{sp} = \alpha_C^{sp} + \beta_C^{sp} G_i + \varepsilon_{iC}^{sp},$$

505 where  $\alpha^{sh}, \alpha_1^{sp}, \dots, \alpha_C^{sp}$  are intercepts.  $G_i \in \{0, 1, 2\}$  is the genotype of individual  $i$ , coded as  
 506 number of minor alleles, and  $\beta^{sh}, \beta_1^{sp}, \dots, \beta_C^{sp}$  are the genetic effects on the shared and each of  
 507 the context-specific expression components. Finally,  $\varepsilon_{i1}^{sp}, \varepsilon_{i1}^{sp}, \dots, \varepsilon_{iC}^{sp}$  are each normally distributed  
 508 residual errors with mean zero and variances  $\sigma_{sh}^2, \sigma_{sp,1}^2, \dots, \sigma_{sp,C}^2$ .

509 Finally, to account for multiple testing across genes, SNPs, and contexts, FastGxC employs  
510 the hierarchical FDR-controlling procedure implemented in [42] (Figure S2). We define a gene-SNP  
511 pair as an eQTL if the SNP has a significant effect on the shared or any of the specific components of  
512 gene expression, i.e., if the global null hypothesis  $H_0 : \beta^{sh} = \beta_1^{sp} = \beta_2^{sp} = \dots = \beta_C^{sp} = 0$  is rejected.  
513 If an eQTL exists, we define a *shared-eQTL* as a variant with a statistically significant effect on  
514 the shared expression component, i.e. if  $H_0 : \beta^{sh} = 0$  is rejected, and a *context-specific eQTL* as  
515 a variant with a statistically significant genetic effect on at least one context-specific expression  
516 components, i.e., if the global null hypothesis  $H_0 : \beta_1^{sp} = \beta_2^{sp} = \dots = \beta_C^{sp} = 0$  is rejected (Figure  
517 S2). In addition, we define a *specific-eQTL in context c* as a variant with a statistically significant  
518 genetic effect on the context-c-specific expression component, i.e., if the marginal null hypothesis  
519  $H_0 : \beta_c^{sp} = 0$  is rejected.

520 **Relationship between FastGxC, CxC, and LM(M)-GxC parameters.** FastGxC's eQTL  
521 effect estimates can be viewed as a computationally efficient reparametrization of those obtained  
522 through CxC and LMM-GxC approaches. Specifically, let  $\beta_c$  represent the eQTL effect in context  $c$ ,  
523 estimated by fitting a linear regression model for each context, i.e.,  $E_{ic} = \alpha_c + \beta_c G_i + \varepsilon_{ic}$ . Then, the  
524 CxC eQTL effect in context  $c$  is equal to the sum of the shared and context-c-specific eQTL effects  
525 from FastGxC, i.e.  $\beta_c = \beta^{sh} + \beta_c^{cs}$ . In addition, let  $\beta_1$  be the eQTL effect in an arbitrarily defined  
526 reference context and  $\delta_c$  be the interaction eQTL effects for the non-reference context  $c$  from an  
527 L(M)M model with a genotype-by-context interaction term, i.e.  $E_{ic} = (u_i) + \alpha + \beta_1 G_i + \sum_{c=2}^C \gamma_c K_{ic} +$   
528  $\sum_{c=2}^C \delta_c G_i \times K_{ic} + \varepsilon_{ic}$ . Then,  $\beta_1 = \beta^{sh} + \beta_1^{cs}$  and  $\delta_c = \beta_c - \beta_1 = \beta^{sh} + \beta_c^{cs} - \beta^{sh} - \beta_1^{cs} = \beta_c^{cs} - \beta_1^{cs}$  for  $c \neq 1$ .  
529 Full details of the analytical derivation are provided in the Supplementary Text.

530 **Simulation study** Genotypes were simulated using a binomial distribution with a minor allele  
531 frequency of 0.2. Gene expression data were generated under 35 scenarios, varying intra-individual  
532 correlation from 0 (independent contexts) to 0.8 and the cis-variant effect in each context (Table  
533 S2). Under the null hypothesis of no context-specific eQTLs (No heterogeneity), the eQTL effect  
534 was either absent across all contexts (No shared eQTL) or identical across contexts (Shared eQTL),  
535 with effect sizes explaining 5% of gene expression variability, consistent with prior estimates of

536 cis-genetic contributions to gene expression heritability [55, 56].

537 Under the alternative hypothesis of eQTL effect size heterogeneity, we simulated three sce-  
538 narios: (i) Single-context heterogeneity, where the eQTL explained 5% of variability in one context  
539 and 0% in others (No shared) or 10% in one context and 5% in others (Shared); (ii) Two-context  
540 heterogeneity, using similar effect size patterns; and (iii) Extensive heterogeneity, where effect sizes  
541 varied across all contexts, ranging from 0% to 10%. For each scenario, we simulated 1,000 datasets.  
542 To assess the impact of sample size, number of contexts, and missing data, we varied the number of  
543 individuals (100 or 698), contexts (8 or 49), and the proportion of missing expression data (approx.  
544 63% and 7% across individuals and contexts), reflecting patterns observed in the GTEx [12] and  
545 OneK1K [15] data.

546 We obtained global estimates of type I error rates and power to identify an eQTL and test  
547 whether the eQTL was context-specific as follows. For the CxC-based approach, we used the  
548 MatrixEQTL R package [57] to fit linear regression models for the effect of the eQTL on expression  
549 in each context  $c$ , i.e.,  $E_{ic} = \alpha_c + \beta_c G_i + \varepsilon_{ic}$ , and obtained  $t$ -test p-values for the null hypothesis  
550 of no eQTL effect in context  $c$ ,  $H_0 : \beta_c = 0$ . Following the hierarchical FDR-controlling procedure  
551 implemented in [42], we then tested the global null hypothesis of no eQTL effect across contexts,  
552  $H_0 : \beta_1 = \dots = \beta_c = 0$ , using Simes's method [58], as implemented in the mppa R package [59], to  
553 combine the  $t$ -test p-values. Global Type I error rate and power to identify an eQTL were computed  
554 as the proportion of datasets in which the eQTL Simes' p-value was significant at the  $\alpha = 5\%$  level.  
555 For the MetaTissue approach, we followed the procedure implemented in [43] and obtained the RE2  
556 p-values which assume no heterogeneity under the null to test the null hypothesis of no eQTL effect.  
557 Global Type I error rate and power to identify a single-context-specific eQTL were computed as the  
558 proportion of datasets in which the  $t$ -test p-value was significant in only one context at  $FDR < 5\%$   
559 for CxC and M-value  $>0.9$  in exactly one context for MetaTissue.

560 We used a similar strategy for FastGxC. Specifically, we fitted linear regression models for the  
561 effect of the eQTL on the shared and each of the  $C$  specific components of expression  $c$ , i.e.,  $E_i^{sh} =$   
562  $\alpha^{sh} + \beta^{sh} G_i + \varepsilon_i^{sh}$  and  $E_{ic}^{sp} = \alpha_c^{sp} + \beta_c^{sp} G_i + \varepsilon_{ic}^{sp}$ , and obtained  $t$ -test p-values for the null hypothesis of  
563 no shared or context- $c$ -specific eQTL effect, i.e.,  $H_0 : \beta^{sh} = 0$  and  $H_0 : \beta_c = 0$ . We then tested the  
564 global null hypothesis of no eQTL effect across contexts,  $H_0 : \beta^{sh} = \beta_1^{sp} = \dots = \beta_C^{sp} = 0$ , and the

565 global null hypothesis of no context-specific eQTL effect in any context,  $H_0 : \beta_1^{sp} = \dots = \beta_C^{sp} = 0$ ,  
566 using Simes' method to combine the corresponding p-values (Figure S2). We computed the global  
567 Type I error rate and power as the proportion of datasets in which the eQTL Simes' p-value was  
568 significant at the  $\alpha = 5\%$  level .

569 Finally, for the LM-GxC approach, we fitted one linear model with a genotype-by-context  
570 interaction term  $E_{ic} = \alpha + \beta G_i + \sum_{c=2}^C \gamma_c K_{ic} + \sum_{c=2}^C \delta_c G_i \times K_{ic} + \varepsilon_{ic}$  and tested the null hypothesis  
571 of no eQTL ( $H_0 : \beta = \delta_2 = \dots = \delta_C = 0$ ) as well as the null hypothesis of no context-specific eQTL  
572 ( $H_0 : \delta_2 = \dots = \delta_C = 0$ ) using likelihood ratio tests (LRT). For the LMM-GxC approach, we fitted  
573 one linear random effects model with a genotype-by-context interaction term  $E_{ic} = u_i + \alpha + \beta G_i +$   
574  $\sum_{c=2}^C \gamma_c K_{ic} + \sum_{c=2}^C \delta_c G_i \times K_{ic} + \varepsilon_{ic}$ ,  $u_i \sim N(0, \sigma_i^2)$  using the `lme4` R package [60] and tested the  
575 same null hypotheses as the LM-GxC model.

576 To assess the ability of FastGxC to identify the heterogeneous context(s), we also obtain  
577 marginal estimates of type I error rate and power within each context by testing  $C$  null hypotheses  
578 of no context-specific eQTL in each context ( $H_0^c : \beta_c^{sp} = 0$ ) using the  $t$ -test implemented in the  
579 `MatrixEQTL` R package [38] and adjust for multiple testing across contexts using the Benjamini-  
580 Hochberg procedure [61]. To compare FastGxC estimates with true simulated effect sizes, we report  
581 the mean effect size across 1,000 simulated datasets for each scenario with a 95% confidence interval  
582 computed as  $\bar{\beta} \pm Z * \frac{\sigma}{\sqrt{n}}$  where  $Z$  is the z-score at  $\alpha = 0.05$ .

583 **GTEX data quality control.** Fully processed, filtered, and normalized gene expression matrices  
584 (in BED format) as well as meta data including genotype PCs, PEER factors, etc (see GTEX paper  
585 [12] for more details) for each tissue across 698 individuals were downloaded through the GTEX  
586 portal (<https://www.gtexportal.org/home/datasets>) on March 11, 2020. Only genes expressed  
587 (as defined by the GTEX consortium [12]) in at least two tissues were considered for downstream  
588 analyses. Prior to eQTL mapping, gene expression matrices were residualized for major sources of  
589 expression variability, including PEER factors, as per the GTEX Consortium [12].

590 WGS genotype VCF data were downloaded from dbGap (dbGaP Accession phs000424.v8.p2),  
591 and only individuals with both genotype and gene expression data were retained (N=698). The VCF  
592 files were processed using `vcftools` (v0.1.16) to retain only bi-allelic SNPs, with variants filtered to

593 include only those with minor allele frequencies greater than 5% in the tissue of interest. Genotype  
594 files were annotated with rs IDs using bcftools (v1.12) [62], and Plink (v1.90) [63] was used to  
595 transpose and convert the VCF files into a sample-by-genotype matrix, which served as input for  
596 eQTL mapping.

597 **OneK1K Genotype QC and Imputation.** Array genotype data for OneK1K was obtained  
598 via the Gene Expression Omnibus (GSE196830) and included genotypes for 1,104 individuals and  
599 759,993 markers on the Illumina Infinium Global Screening Array. For downstream analyses, only  
600 individuals with gene expression data were considered ( $N = 981$ ). Bcftools version 1.18 was used  
601 to map SNPs to the GRCh37.13 build 151 of dbSNP [64] and adjust allele strand orientation for  
602 mismatches. PLINK version 1.90 [63] was used to filter SNPs and individuals with a call rate  
603 less than 0.95 (zero individuals and 11,317 SNPs), SNPs with a Hardy-Weinberg equilibrium test  
604 p-value less than  $10^{-6}$  (1,857 SNPs), minor allele frequency (MAF) below 0.01 (211,894 SNPs), and  
605 individuals with ambiguous sex labeling (one individual).

606 To identify ancestry outlier samples, we performed principal component analysis (PCA) jointly  
607 on the OneK1K and 1000 Genome Phase I samples. 1000 Genome Phase I data was downloaded  
608 from the EMBL-EBI public endpoint (<http://ftp.ebi.ac.uk/1000g/ftp/>). PCA was conducted  
609 on the merged data using PLINK version 2.0, and 3 individuals with non-European ancestry, defined  
610 as being within three standard deviations from the European mean of genetic principal components  
611 1 and 2, were excluded. Excess autosomal heterozygosity, defined as being within three standard  
612 deviations from the mean, was computed with PLINK version 1.90 and 7 individuals were removed.  
613 A genetic relationship matrix from all autosomal SNPs was generated using KING version 2.3.1  
614 [65]. No individuals were excluded based on a 0.125 relatedness threshold (second-degree relatives).

615 After quality control, 499,909 autosomal SNPs from 970 individuals were retained for im-  
616 putation. Imputation was performed using the Michigan Imputation Server [66] with the 1000G  
617 phase III V5 reference panel [67] and was run using Minimac4 and Eagle v2.4. For subsequent  
618 cis-eQTL analyses, 5,849,361 SNPs with imputation quality R-squared of at least 0.8 and a minor  
619 allele frequency above 0.05 were retained.

620 **CLUES Genotype QC and Imputation.** Genotype data for 237 individuals (188 labeled  
621 as SLE and 49 labeled as Immvar) from CLUES was obtained from dbGap (accession number  
622 phs002812.v1.p1). Genotypes from the SLE and Immvar CLUES cohorts were processed and im-  
623 puted separately, as in [14], resulting in 22,159,030 variants for the SLE cohort and 9,797,072 variants  
624 for the Immvar cohort. After imputation, variants with an imputation quality R-squared greater  
625 than 0.8 were retained, and the datasets were merged using PLINK v2.0, producing a combined  
626 total of 16,616,859 variants.

627 Based on genetically determined ancestry, individuals were then split into European (N=140)  
628 and Asian (N=97) cohorts, following the approach described in Perez et al [14]. Within each  
629 ancestry group, PLINK v2.0 was used to filter for variants with a minor allele frequency above 5%,  
630 resulting in 4,995,061 variants in the Asian cohort and 5,292,554 variants in the European cohort for  
631 further analysis. Genotype principal components were computed within each cohort using PLINK  
632 v1.90 to identify outlier individuals, defined as those within three standard deviations of the mean  
633 for genetic principal components 1 and 2. This filtering excluded 5 individuals from the Asian  
634 cohort and 8 from the European cohort.

635 **OneK1K and CLUES Gene Expression QC.** Gene expression data for the CLUES cohort  
636 was obtained from GEO (accession number GSE174188). For downstream analysis, we retained cells  
637 from the eight cell types used for cis-eQTL analysis in [14]: B cells, conventional and plasmacytoid  
638 dendritic cells (cDC and pDC), classical and non-classical monocytes (cMono and ncMono), NK  
639 cells, CD4 T cells, and CD8 T cells. As with genotype data, the CLUES cohort was divided into  
640 European and Asian ancestry groups. Only individuals with both expression and genotypes were  
641 retained, i.e., N=140 and N=97 European and Asian ancestry individuals.

642 Gene expression data for the OneK1K cohort was obtained via GEO (accession number  
643 GSE196830). From the 29 pre-defined cell type clusters, we consolidated labels for similar cell  
644 types. Specifically, memory B cells, naive B cells, and transitional B cells were grouped as B cells;  
645 natural killer cells and CD16-negative, CD56-bright natural killer cells were combined as NK cells;  
646 T alpha-beta cytotoxic, CD4-positive cells, T alpha-beta, CD4-positive cells, and T regulatory cells  
647 were grouped as CD4 T cells; and T alpha-beta, CD8-positive cells, T gamma-delta cells, and T

648 mucosal invariant cells were grouped as CD8 T cells. For downstream analyses, only cells from the  
649 eight cell types present in CLUES were retained. In addition, only individuals with both expression  
650 and genotypes were retained, i.e., N=981 individuals.

651 For each individual in the CLUES European, CLUES Asian, and OneK1K cohorts, a pseudo-  
652 bulk expression profile was generated by averaging counts across cells for each cell type and gene.  
653 The following steps were then applied separately within each cohort and cell type. First, expression  
654 values for each gene were adjusted for library size factors and normalized using counts per million  
655 (CPM) and transcripts per million (TPM). Genes with normalized expression greater than zero in at  
656 least 10% of samples were retained. Gene expression values were then transformed to approximate  
657 normality using the `RankNorm` function in the `RNOmni` R package [68]. Within each cohort, genes  
658 expressed in fewer than three cell types were excluded. Next, principal component analysis (PCA)  
659 was applied to identify and remove outlier samples defined as those falling outside three standard  
660 deviations from the mean of expression principal components 1 and 2. After quality control, 17,199,  
661 16,225, and 14,701 genes and 132, 92, and 970 individuals in the CLUES European, CLUES Asian,  
662 and OneK1K cohorts, respectively, were retained for downstream analyses.

663 To capture major sources of expression variation, the PCA implementation in the `PCAForQTL`  
664 R package [69] was used with the `runBE` function to determine the number of principal components  
665 that explain a significant portion of variation in each cell type. Gene expression data for each  
666 cell type and cohort was then residualized for six genotype principal components, selected gene  
667 expression principal components, sex, age, batch, and, in CLUES cohorts only, SLE status.

668 **Expression principal components analysis and correlation with covariates.** To evaluate  
669 the effectiveness of FastGxC in removing gene expression background noise, we first applied PCA  
670 separately to the original gene expression data and the decomposed shared and context-specific  
671 expression data, using the `prcomp` function in the `stats` R package. Next, we correlated technical  
672 and biological covariates with the first ten principal components (PCs) from each data. The corre-  
673 lation between expression PCs and covariates was computed using the `canCorPairs` function from  
674 the `variancePartition` R package ([70]). In short, when comparing two continuous variables (e.g.  
675 gPC1 or weight), Pearson correlation was used. In order to accommodate the correlation between a

676 continuous and a categorical variable (e.g. cohort) canonical correlation analysis (CCA) was used.  
677 Note that CCA returns correlations values between 0 and 1.

678 **FastGxC and CxC eQTL mapping.** Residualized gene expression (see methods above) for  
679 each was mean-centered across all individuals and contexts, then decomposed into 49 tissue-specific  
680 components for GTEx and 8 -cell type-specific components for CLUES and OneK1K, along with one  
681 shared expression component. Cis genetic effects were estimated on shared gene expression levels  
682 (FastGxC), context-specific gene expression levels (FastGxC), and gene expression levels within  
683 each context (CxC) using ultra-fast linear regression models in the `MatrixEQTL` R package [38],  
684 with `model=modellINEAR` and a 1 Mb window for cis-eQTL calls. The CLUES European, CLUES  
685 Asian, and OneK1K cohorts were then meta-analyzed within each cell type using METASOFT  
686 (v2.0) [71] random effect model (RE2) with default parameters.

687 Multiple testing correction was applied separately for CxC and FastGxC and for bulk and  
688 meta-analyzed single-cell results using the hierarchical FDR procedures in the `TreeQTL` R package  
689 [42] with an alpha level of 5% in each level. For the CxC approach, a three-level hierarchy with  
690 genes, gene-SNP pairs, and gene-SNP-context triplets was used . For FastGxC, multiple testing  
691 correction was applied separately for the shared and specific components using a two-level hierarchy  
692 for shared eQTLs (genes and gene-SNP pairs) and a three-level hierarchy for context-specific eQTLs  
693 (genes, gene-SNP pairs, and gene-SNP-context triplets) (Figure S2B).

694 **Correlations of eQTL effect sizes across context.** Pearson correlations were computed across  
695 all tissues in GTEx using effect sizes of only the significant eQTLs in each tissue for the CxC  
696 approach or tissue-specific eQTLs for FastGxC. Missing effect size values, due to an eQTL not  
697 being tested or not reaching significance in some tissues, were set to zero, and pairwise complete  
698 correlations were calculated using the `cor` function in R. For single PBMC cell types, Pearson  
699 correlations of eQTL effect sizes across cell types were computed using all tested, meta-analyzed  
700 METASOFT RE2 effect sizes.

701 **Building set of background SNP for enrichment analyses** The `matchit` function from  
702 the `MatchIt` R package was used to create a set of background SNP-gene pairs for each variant

703 set of interest, matched by minor allele frequency (MAF) using the nearest neighbor matching  
704 method with a 1:1 ratio [72]. Only variants used for eQTL mapping were included in building  
705 these background sets. For eQTL sets containing more than 5,000 variants, the sets were randomly  
706 split into chunks to expedite computation. This analysis was done separately in bulk-tissues and  
707 single-cell PBMCs and for FastGxC and CxC eQTLs.

708 **EQTL enrichment in genomic features** To test for enrichment of various eQTL types within  
709 genomic annotations, we first created variant sets specific to each type of eQTL. This analysis  
710 was conducted separately for bulk tissues and single-cell PBMC cell types. Specific-eQTL-only  
711 and shared-eQTL-only variant sets were derived by taking the set difference of specific-eQTL and  
712 shared-eQTL variants. The FastGxC eQTL variant set was constructed by combining shared- and  
713 specific-eQTL variants across contexts, and the CxC eQTL variant set was created by taking the  
714 union of eQTL variants across contexts. We then calculated the set difference between the FastGxC  
715 and CxC eQTL variant sets to obtain the final FastGxC-only and CxC-only eQTL variant sets.

716 Variants from each set were annotated using the Ensembl Variant Effect Predictor (VEP) tool,  
717 which identifies variant effects, such as potential impacts on protein sequences or positioning within  
718 genomic regulatory elements. Enrichment of each eQTL set within VEP-annotated categories was  
719 tested using a one-sided Fisher's exact test from the `stats` R package, followed by BH correction;  
720 significance was defined as a BH-adjusted p-value less than 0.05.

721 **Enrichment in regions of open chromatin** For bulk tissues, all available tissue ATAC-seq  
722 data in the 'not perturbed,' GRCh38, and bigBed narrowPeak categories were downloaded from  
723 [www.encodeproject.org](http://www.encodeproject.org) in November 2020. The downloaded bigBed files were converted to  
724 bed format using the UCSC `bigbedtobed` tool for downstream analysis. For single-cell PBMC  
725 cell types, cell-type-specific ATAC-seq peaks were downloaded from [https://web.stanford.edu/group/pritchardlab/dataArchive/immune\\_atlas\\_web/index.html](https://web.stanford.edu/group/pritchardlab/dataArchive/immune_atlas_web/index.html) [21] and grouped into major  
726 cell types (B, T, NK, Myeloid, Open), following the approach of Perez et al. [14]. Bed files were then  
727 sorted using the command `bedtools sort -k1,1 -k2,2n` to enable memory-efficient processing for  
728 subsequent intersections.

730 Enrichment analysis of FastGxC and CxC single-context eQTL variants from both bulk tis-  
731 sues and single-cell PBMC cell types in regions of open chromatin was performed by intersecting  
732 each eQTL variant set of interest with each pre-sorted bed file, representing ATAC-seq peaks from  
733 a tissue, cell type, or sample (when multiple samples were available for each context), using the  
734 `bedtools intersectBed` command. A one-sided Fisher's exact test was used to obtain the statis-  
735 tical significance of each enrichment, followed by BH multiple testing adjustment. Significance was  
736 called for BH-adjusted p-values less than 0.05.

737 **Enrichment of bulk tissue eQTLs in GWAS loci** Genome-wide association study (GWAS)  
738 data ([gwas\\_catalog\\_v1.0.2-associations\\_e100\\_r2020-06-17](#)) including 1,563 unique traits was  
739 downloaded from the NHGRI-EBI GWAS Catalog in August 2020 [\[48\]](#) and processed for down-  
740 stream analysis. Matching of variants with and without eQTL effects was performed as previously  
741 described.

742 Enrichment analysis of FastGxC and CxC eQTL variants was performed by intersecting each  
743 eQTL variant set of interest with trait-associated variants from the GWAS catalog based on rs IDs.  
744 Statistical significance was assessed using a one-sided Fisher's exact test for each enrichment. Only  
745 mapped traits within the GWAS catalog that contained at least 10 significant loci were included in  
746 our downstream analysis resulting in 539 traits with complete enrichment results. Multiple testing  
747 correction was applied using the hierarchical FDR procedures in the TreeQTL R package [\[42\]](#), with  
748 tissues at level one and tissue-trait pairs at level two, maintaining an FDR of 5% at each level.

749 The most likely causal tissue(s) for the 539 GWAS traits were annotated manually, following  
750 the approach used in [\[12\]](#). These annotations were used to calculate precision and recall rates.  
751 Specifically, for each trait, a contingency table was constructed to capture the frequency with which  
752 a trait of interest is both enriched in a tissue's eQTLs and assigned as the likely relevant tissue.  
753 This yielded true positive, false positive, true negative, and false negative counts (TP, FP, TN, FN).  
754 Precision was calculated as  $TP / (TP + FP)$ , and recall as  $TP / (TP + FN)$ .

755 **Colocalization of eQTLs with GWAS variants** We obtained complete GWAS summary  
756 statistics for 63 unique complex traits. The list of traits analyzed, along with their references,

757 is available in Table S5. Colocalization analysis of GWAS variants with eQTLs from bulk tissues  
758 and single-cell PBMC cell types was conducted using a custom integration of FINEMAP [73] and  
759 eCAVIAR [74] with an LD-modified colocalization posterior probability ( $CLPP_{mod}$ ) following the  
760 method outlined in Gloudemans et al. [13]. Significant colocalization was defined as  $CLPP_{mod}$   
761 above 0.5, as in [75], and impact of this threshold on results is studied in Figure S20. To assess the  
762 colocalization contribution from FastGxC specific versus shared eQTLs in PBMCs, we limited our  
763 analysis to the 10 immune related traits out of the original 63.

## 867 References

868 [1] Elliot Sollis, Abayomi Mosaku, et al. “The NHGRI-EBI GWAS Catalog: knowledgebase and  
869 deposition resource”. In: *Nucleic Acids Research* 51.D1 (Nov. 2022), D977–D985. ISSN: 1362-  
870 4962. DOI: [10.1093/nar/gkac1010](https://doi.org/10.1093/nar/gkac1010). URL: <http://dx.doi.org/10.1093/nar/gkac1010>.

871 [2] Matthew T. Maurano, Richard Humbert, et al. “Systematic Localization of Common Disease-  
872 Associated Variation in Regulatory DNA”. In: *Science (New York, N.Y.)* 337.6099 (Sept. 7,  
873 2012), pp. 1190–1195. ISSN: 0036-8075. DOI: [10.1126/science.1222794](https://doi.org/10.1126/science.1222794). URL: <https://www.ncbi.nlm.nih.gov/pmc/articles/PMC3771521/> (visited on 04/23/2021).

874 [3] Dan L. Nicolae, Eric Gamazon, et al. “Trait-Associated SNPs Are More Likely to Be eQTLs:  
875 Annotation to Enhance Discovery from GWAS”. In: *PLoS Genetics* 6.4 (Apr. 2010). Ed.  
876 by Greg Gibson, e1000888. ISSN: 1553-7404. DOI: [10.1371/journal.pgen.1000888](https://doi.org/10.1371/journal.pgen.1000888). URL:  
877 <http://dx.doi.org/10.1371/journal.pgen.1000888>.

878 [4] Alexander Gusev, S. Hong Lee, et al. “Partitioning Heritability of Regulatory and Cell-Type-  
879 Specific Variants across 11 Common Diseases”. In: *The American Journal of Human Genetics*  
880 95.5 (Nov. 2014), 535–552. ISSN: 0002-9297. DOI: [10.1016/j.ajhg.2014.10.004](https://doi.org/10.1016/j.ajhg.2014.10.004). URL: <http://dx.doi.org/10.1016/j.ajhg.2014.10.004>.

881 [5] Eric R. Gamazon, Ayellet V. Segrè, et al. “Using an atlas of gene regulation across 44 human  
882 tissues to inform complex disease- and trait-associated variation”. In: *Nature Genetics* 50.7  
883 (July 2018), pp. 956–967. ISSN: 1546-1718. DOI: [10.1038/s41588-018-0154-4](https://doi.org/10.1038/s41588-018-0154-4). URL: <https://www.nature.com/articles/s41588-018-0154-4> (visited on 04/26/2021).

884 [6] Mete Civelek, Ying Wu, et al. “Genetic Regulation of Adipose Gene Expression and Cardio-  
885 Metabolic Traits”. In: *The American Journal of Human Genetics* 100.3 (Mar. 2017), 428–443.  
886 ISSN: 0002-9297. DOI: [10.1016/j.ajhg.2017.01.027](https://doi.org/10.1016/j.ajhg.2017.01.027). URL: <http://dx.doi.org/10.1016/j.ajhg.2017.01.027>.

887 [7] “Identification of an imprinted master trans regulator at the KLF14 locus related to multiple  
888 metabolic phenotypes”. In: *Nature Genetics* 43.6 (May 2011), 561–564. ISSN: 1546-1718. DOI:  
889 [10.1038/ng.833](https://doi.org/10.1038/ng.833). URL: <http://dx.doi.org/10.1038/ng.833>.

894 [8] Simon Koplev, Marcus Seldin, et al. “A mechanistic framework for cardiometabolic and coro-  
895 nary artery diseases”. In: *Nature Cardiovascular Research* 1.1 (Jan. 2022), 85–100. ISSN: 2731-  
896 0590. DOI: [10.1038/s44161-021-00009-1](https://doi.org/10.1038/s44161-021-00009-1). URL: <http://dx.doi.org/10.1038/s44161-021-00009-1>.

897 [9] Philip L. De Jager, Yiyi Ma, et al. “A multi-omic atlas of the human frontal cortex for aging  
898 and Alzheimer’s disease research”. In: *Scientific Data* 5.1 (Aug. 2018). ISSN: 2052-4463. DOI:  
900 [10.1038/sdata.2018.142](https://doi.org/10.1038/sdata.2018.142). URL: <http://dx.doi.org/10.1038/sdata.2018.142>.

901 [10] Masashi Fujita, Zongmei Gao, et al. “Cell subtype-specific effects of genetic variation in the  
902 Alzheimer’s disease brain”. In: *Nature Genetics* 56.4 (Mar. 2024), 605–614. ISSN: 1546-1718.  
903 DOI: [10.1038/s41588-024-01685-y](https://doi.org/10.1038/s41588-024-01685-y). URL: <http://dx.doi.org/10.1038/s41588-024-01685-y>.

904 [11] Peter Orchard, Thomas W. Blackwell, et al. “Cross-cohort analysis of expression and splicing  
905 quantitative trait loci in TOPMed”. In: (Feb. 2025). DOI: [10.1101/2025.02.19.25322561](https://doi.org/10.1101/2025.02.19.25322561).  
906 URL: <http://dx.doi.org/10.1101/2025.02.19.25322561>.

907 [12] The GTEx Consortium. “The GTEx Consortium atlas of genetic regulatory effects across  
908 human tissues”. In: *Science* 369.6509 (Sept. 11, 2020). Publisher: American Association for  
909 the Advancement of Science Section: Research Article, pp. 1318–1330. ISSN: 0036-8075, 1095-  
910 9203. DOI: [10.1126/science.aaz1776](https://doi.org/10.1126/science.aaz1776). URL: <https://science.science.org/content/369/6509/1318> (visited on 11/04/2020).

911 [13] Michael J. Gloudemans, Brunilda Balliu, et al. “Integration of genetic colocalizations with  
912 physiological and pharmacological perturbations identifies cardiometabolic disease genes”. In:  
913 *Genome Medicine* 14.1 (Mar. 2022). ISSN: 1756-994X. DOI: [10.1186/s13073-022-01036-8](https://doi.org/10.1186/s13073-022-01036-8).  
914 URL: <http://dx.doi.org/10.1186/s13073-022-01036-8>.

915 [14] Richard K. Perez, M. Grace Gordon, et al. “Single-cell RNA-seq reveals cell type-specific  
916 molecular and genetic associations to lupus”. In: *Science* 376.6589 (Apr. 8, 2022). Publisher:  
917 American Association for the Advancement of Science, eabf1970. DOI: [10.1126/science.abf1970](https://doi.org/10.1126/science.abf1970). URL: <https://www.science.org/doi/10.1126/science.abf1970> (visited on  
918 11/23/2022).

919

920

921

922 [15] Seyhan Yazar, Jose Alquicira-Hernandez, et al. “Single-cell eQTL mapping identifies cell  
923 type-specific genetic control of autoimmune disease”. In: *Science* 376.6589 (Apr. 8, 2022).  
924 Publisher: American Association for the Advancement of Science, eabf3041. doi: [10.1126/science.abf3041](https://doi.org/10.1126/science.abf3041). URL: <https://www.science.org/doi/10.1126/science.abf3041>  
925 (visited on 11/23/2022).

927 [16] Benjamin D. Umans, Alexis Battle, and Yoav Gilad. “Where Are the Disease-Associated  
928 eQTLs?” In: *Trends in Genetics* 37.2 (Feb. 1, 2021), pp. 109–124. ISSN: 0168-9525. doi:  
929 [10.1016/j.tig.2020.08.009](https://doi.org/10.1016/j.tig.2020.08.009). URL: <https://www.sciencedirect.com/science/article/pii/S0168952520302092> (visited on 04/26/2021).

931 [17] Noah J Connally, Sumaiya Nazeen, et al. “The missing link between genetic association and  
932 regulatory function”. In: *eLife* 11 (Dec. 2022). ISSN: 2050-084X. doi: [10.7554/elife.74970](https://doi.org/10.7554/elife.74970).  
933 URL: [http://dx.doi.org/10.7554/elife.74970](https://doi.org/10.7554/elife.74970).

934 [18] Hakhamanesh Mostafavi, Jeffrey P. Spence, et al. “Systematic differences in discovery of  
935 genetic effects on gene expression and complex traits”. In: *Nature Genetics* 55.11 (Oct. 2023),  
936 1866–1875. ISSN: 1546-1718. doi: [10.1038/s41588-023-01529-1](https://doi.org/10.1038/s41588-023-01529-1). URL: [http://dx.doi.org/10.1038/s41588-023-01529-1](https://doi.org/10.1038/s41588-023-01529-1).

938 [19] Benjamin P. Fairfax, Peter Humburg, et al. “Innate Immune Activity Conditions the Effect of  
939 Regulatory Variants upon Monocyte Gene Expression”. In: *Science* 343.6175 (Mar. 7, 2014).  
940 Publisher: American Association for the Advancement of Science Section: Research Article.  
941 ISSN: 0036-8075, 1095-9203. doi: [10.1126/science.1246949](https://doi.org/10.1126/science.1246949). URL: <https://science.org/sciencemag.org/content/343/6175/1246949> (visited on 11/04/2020).

943 [20] Chun Jimmie Ye, Jenny Chen, et al. “Genetic analysis of isoform usage in the human anti-viral  
944 response reveals influenza-specific regulation of ERAP2 transcripts under balancing selection”.  
945 en. In: *Genome Research* 28.12 (Dec. 2018), pp. 1812–1825. ISSN: 1088-9051, 1549-5469. doi:  
946 [10.1101/gr.240390.118](https://doi.org/10.1101/gr.240390.118). URL: <https://genome.cshlp.org/content/28/12/1812> (visited  
947 on 04/23/2021).

948 [21] Diego Calderon, Michelle L. T. Nguyen, et al. “Landscape of stimulation-responsive chromatin  
949 across diverse human immune cells”. In: *Nature Genetics* 51.10 (Sept. 2019), 1494–1505. ISSN:

950 1546-1718. DOI: [10.1038/s41588-019-0505-9](https://doi.org/10.1038/s41588-019-0505-9). URL: <http://dx.doi.org/10.1038/s41588-019-0505-9>.

951

952 [22] Maria Gutierrez-Arcelus, Yuriy Baglaenko, et al. “Allele-specific expression changes dynamically during T cell activation in HLA and other autoimmune loci”. In: *Nature Genetics* 52.3 (Feb. 2020), 247–253. ISSN: 1546-1718. DOI: [10.1038/s41588-020-0579-4](https://doi.org/10.1038/s41588-020-0579-4). URL: <http://dx.doi.org/10.1038/s41588-020-0579-4>.

953

954

955

956 [23] Nana Matoba, Brandon D. Le, et al. “Stimulating Wnt signaling reveals context-dependent genetic effects on gene regulation in primary human neural progenitors”. In: *Nature Neuroscience* 27.12 (Sept. 2024), 2430–2442. ISSN: 1546-1726. DOI: [10.1038/s41593-024-01773-6](https://doi.org/10.1038/s41593-024-01773-6). URL: <http://dx.doi.org/10.1038/s41593-024-01773-6>.

957

958

959

960 [24] Benjamin J. Strober, Karl Tayeb, et al. “SURGE: uncovering context-specific genetic-regulation of gene expression from single-cell RNA sequencing using latent-factor models”. In: *Genome Biology* 25.1 (Jan. 2024). ISSN: 1474-760X. DOI: [10.1186/s13059-023-03152-z](https://doi.org/10.1186/s13059-023-03152-z). URL: <http://dx.doi.org/10.1186/s13059-023-03152-z>.

961

962

963

964 [25] Anna S E Cuomo, Tobias Heinen, et al. “CellRegMap: a statistical framework for mapping context-specific regulatory variants using scRNA-seq”. In: *Molecular Systems Biology* 18.8 (Aug. 2022). Publisher: John Wiley & Sons, Ltd, e10663. ISSN: 1744-4292. DOI: [10.15252/msb.202110663](https://doi.org/10.15252/msb.202110663). URL: <https://www.embopress.org/doi/full/10.15252/msb.202110663> (visited on 11/23/2022).

965

966

967

968

969 [26] Wancen Mu, Hirak Sarkar, et al. “Airport: interpretable statistical models for analyzing allelic imbalance in single-cell datasets”. In: *Bioinformatics* 38.10 (Apr. 2022). Ed. by Christina Kendziorski, 2773–2780. ISSN: 1367-4811. DOI: [10.1093/bioinformatics/btac212](https://doi.org/10.1093/bioinformatics/btac212). URL: <http://dx.doi.org/10.1093/bioinformatics/btac212>.

970

971

972

973 [27] Tobias Heinen, Stefano Secchia, et al. “scDALI: modeling allelic heterogeneity in single cells reveals context-specific genetic regulation”. In: *Genome Biology* 23.1 (Jan. 6, 2022), p. 8. ISSN: 1474-760X. DOI: [10.1186/s13059-021-02593-8](https://doi.org/10.1186/s13059-021-02593-8). URL: <https://doi.org/10.1186/s13059-021-02593-8> (visited on 11/23/2022).

974

975

976

977 [28] Guanghao Qi, Benjamin J. Strober, et al. “Single-cell allele-specific expression analysis reveals  
978 dynamic and cell-type-specific regulatory effects”. In: *Nature Communications* 14.1 (Oct.  
979 2023). ISSN: 2041-1723. DOI: [10.1038/s41467-023-42016-9](https://doi.org/10.1038/s41467-023-42016-9). URL: <http://dx.doi.org/10.1038/s41467-023-42016-9>.

980

981 [29] Lingfei Wang. “Airqlt dissects cell state-specific causal gene regulatory networks with efficient  
982 single-cell eQTL mapping”. In: *bioRxiv* (Jan. 2025). DOI: [10.1101/2025.01.15.633041](https://doi.org/10.1101/2025.01.15.633041). URL:  
983 <http://dx.doi.org/10.1101/2025.01.15.633041>.

984 [30] Natsuhiko Kumashita, Raghd Rostom, et al. “Mapping interindividual dynamics of innate  
985 immune response at single-cell resolution”. In: *Nature Genetics* 55.6 (June 2023), 1066–1075.  
986 ISSN: 1546-1718. DOI: [10.1038/s41588-023-01421-y](https://doi.org/10.1038/s41588-023-01421-y). URL: <http://dx.doi.org/10.1038/s41588-023-01421-y>.

987

988 [31] Wei Zhou, Anna S.E. Cuomo, et al. “Efficient and accurate mixed model association tool for  
989 single-cell eQTL analysis”. In: *medRxiv* (May 2024). DOI: [10.1101/2024.05.15.24307317](https://doi.org/10.1101/2024.05.15.24307317).  
990 URL: <http://dx.doi.org/10.1101/2024.05.15.24307317>.

991 [32] Benjamin J. Schmiedel, Divya Singh, et al. “Impact of Genetic Polymorphisms on Human  
992 Immune Cell Gene Expression”. In: *Cell* 175.6 (Nov. 2018), 1701–1715.e16. ISSN: 0092-8674.  
993 DOI: [10.1016/j.cell.2018.10.022](https://doi.org/10.1016/j.cell.2018.10.022). URL: <http://dx.doi.org/10.1016/j.cell.2018.10.022>.

994

995 [33] Zixuan Eleanor Zhang, Artem Kim, et al. “Efficient count-based models improve power and  
996 robustness for large-scale single-cell eQTL mapping”. In: *bioRxiv* (Jan. 2025). DOI: [10.1101/2025.01.18.25320755](https://doi.org/10.1101/2025.01.18.25320755). URL: <http://dx.doi.org/10.1101/2025.01.18.25320755>.

997

998 [34] Sarah M. Urbut, Gao Wang, et al. “Flexible statistical methods for estimating and testing  
999 effects in genomic studies with multiple conditions”. en. In: *Nature Genetics* 51.1 (Jan. 2019),  
1000 pp. 187–195. ISSN: 1546-1718. DOI: [10.1038/s41588-018-0268-8](https://doi.org/10.1038/s41588-018-0268-8). URL: <https://www.nature.com/articles/s41588-018-0268-8> (visited on 09/11/2020).

1001

1002 [35] Kimberly R. Kukurba, Princy Parsana, et al. “Impact of the X Chromosome and sex on  
1003 regulatory variation”. In: *Genome Research* 26.6 (June 2016), pp. 768–777. ISSN: 1549-5469.  
1004 DOI: [10.1101/gr.197897.115](https://doi.org/10.1101/gr.197897.115).

1005 [36] Brunilda Balliu, Matthew Durrant, et al. “Genetic regulation of gene expression and splicing  
1006 during a 10-year period of human aging”. In: *Genome Biology* 20.1 (Nov. 2019), p. 230. ISSN:  
1007 1474-760X. DOI: [10.1186/s13059-019-1840-y](https://doi.org/10.1186/s13059-019-1840-y). URL: <https://doi.org/10.1186/s13059-019-1840-y> (visited on 09/10/2020).

1009 [37] Meritxell Oliva, Manuel Muñoz-Aguirre, et al. “The impact of sex on gene expression across  
1010 human tissues”. In: *Science* 369.6509 (Sept. 11, 2020). ISSN: 0036-8075, 1095-9203. DOI: [10.1126/science.aba3066](https://doi.org/10.1126/science.aba3066). URL: <https://science.scienmag.org/content/369/6509/aba3066> (visited on 04/16/2021).

1013 [38] Andrey A. Shabalin. “Matrix eQTL: ultra fast eQTL analysis via large matrix operations”.  
1014 eng. In: *Bioinformatics (Oxford, England)* 28.10 (May 2012), pp. 1353–1358. ISSN: 1367-4811.  
1015 DOI: [10.1093/bioinformatics/bts163](https://doi.org/10.1093/bioinformatics/bts163).

1016 [39] Amaro Taylor-Weiner, François Aguet, et al. “Scaling computational genomics to millions  
1017 of individuals with GPUs”. In: *Genome Biology* 20.1 (Nov. 2019). ISSN: 1474-760X. DOI:  
1018 [10.1186/s13059-019-1836-7](https://doi.org/10.1186/s13059-019-1836-7). URL: <http://dx.doi.org/10.1186/s13059-019-1836-7>.

1019 [40] Olivier Delaneau, Halit Ongen, et al. “A complete tool set for molecular QTL discovery  
1020 and analysis”. In: *Nature Communications* 8.1 (May 2017). ISSN: 2041-1723. DOI: [10.1038/ncomms15452](https://doi.org/10.1038/ncomms15452). URL: <http://dx.doi.org/10.1038/ncomms15452>.

1022 [41] Patrick J. Potvin and Robert W. Schutz. “Statistical power for the two-factor repeated mea-  
1023 sures ANOVA”. In: *Behavior Research Methods, Instruments, & Computers* 32.2 (June  
1024 2000), 347–356. ISSN: 1532-5970. DOI: [10.3758/bf03207805](https://doi.org/10.3758/bf03207805). URL: <http://dx.doi.org/10.3758/BF03207805>.

1026 [42] C. B. Peterson, M. Bogomolov, et al. “TreeQTL: hierarchical error control for eQTL findings”.  
1027 In: *Bioinformatics (Oxford, England)* 32.16 (Aug. 15, 2016), pp. 2556–2558. ISSN: 1367-4811.  
1028 DOI: [10.1093/bioinformatics/btw198](https://doi.org/10.1093/bioinformatics/btw198).

1029 [43] Jae Hoon Sul, Buhm Han, et al. “Effectively Identifying eQTLs from Multiple Tissues by Com-  
1030 bining Mixed Model and Meta-analytic Approaches”. In: *PLOS Genetics* 9.6 (June 13, 2013).  
1031 Publisher: Public Library of Science, e1003491. ISSN: 1553-7404. DOI: [10.1371/journal.pgen.1003491](https://doi.org/10.1371/journal.pgen.1003491). URL: <https://journals.plos.org/plosgenetics/article?id=10.1371/journal.pgen.1003491> (visited on 04/02/2021).

1034 [44] Timothy D. Arthur, Jennifer P. Nguyen, et al. “Multi-omic QTL mapping in early develop-  
1035 mental tissues reveals phenotypic and temporal complexity of regulatory variants underlying  
1036 GWAS loci”. In: *bioRxiv* (Apr. 2024). DOI: [10.1101/2024.04.10.588874](https://doi.org/10.1101/2024.04.10.588874). URL: [http://dx.doi.org/10.1101/2024.04.10.588874](https://doi.org/10.1101/2024.04.10.588874).

1038 [45] D. S. Gross and W. T. Garrard. “Nuclease hypersensitive sites in chromatin”. In: *Annual  
1039 Review of Biochemistry* 57 (1988), pp. 159–197. ISSN: 0066-4154. DOI: [10.1146/annurev.bi.57.070188.001111](https://doi.org/10.1146/annurev.bi.57.070188.001111).

1041 [46] Igor Mandric, Jeremy Rotman, et al. “Profiling immunoglobulin repertoires across multiple  
1042 human tissues using RNA sequencing”. In: *Nature Communications* 11.1 (Dec. 2020), p. 3126.  
1043 ISSN: 2041-1723. DOI: [10.1038/s41467-020-16857-7](https://doi.org/10.1038/s41467-020-16857-7). URL: <http://www.nature.com/articles/s41467-020-16857-7> (visited on 05/10/2021).

1045 [47] Serghei Mangul, Harry Taegyun Yang, et al. “ROP: dumpster diving in RNA-sequencing to  
1046 find the source of 1 trillion reads across diverse adult human tissues”. In: *Genome Biology*  
1047 19.1 (Feb. 15, 2018), p. 36. ISSN: 1474-760X. DOI: [10.1186/s13059-018-1403-7](https://doi.org/10.1186/s13059-018-1403-7). URL:  
1048 <https://doi.org/10.1186/s13059-018-1403-7> (visited on 05/10/2021).

1049 [48] Annalisa Buniello, Jacqueline A. L. MacArthur, et al. “The NHGRI-EBI GWAS Catalog of  
1050 published genome-wide association studies, targeted arrays and summary statistics 2019”.  
1051 In: *Nucleic Acids Research* 47 (D1 Jan. 8, 2019), pp. D1005–D1012. ISSN: 1362-4962. DOI:  
1052 [10.1093/nar/gky1120](https://doi.org/10.1093/nar/gky1120).

1053 [49] Anna S. E. Cuomo, Giordano Alvari, et al. “Optimizing expression quantitative trait locus  
1054 mapping workflows for single-cell studies”. In: *Genome Biology* 22.1 (June 2021). ISSN: 1474-  
1055 760X. DOI: [10.1186/s13059-021-02407-x](https://doi.org/10.1186/s13059-021-02407-x). URL: <http://dx.doi.org/10.1186/s13059-021-02407-x>.

1057 [50] Silvia Domcke and Jay Shendure. “A reference cell tree will serve science better than a  
1058 reference cell atlas”. In: *Cell* 186.6 (Mar. 16, 2023), pp. 1103–1114. ISSN: 0092-8674. DOI:  
1059 [10.1016/j.cell.2023.02.016](https://doi.org/10.1016/j.cell.2023.02.016). URL: <https://www.sciencedirect.com/science/article/pii/S0092867423001599> (visited on 08/28/2024).

1060

1061 [51] Mike Thompson, Mary Grace Gordon, et al. “Multi-context genetic modeling of transcrip-  
1062 tional regulation resolves novel disease loci”. In: *Nature Communications* 13.1 (Sept. 2022).  
1063 ISSN: 2041-1723. DOI: [10.1038/s41467-022-33212-0](https://doi.org/10.1038/s41467-022-33212-0), URL: <http://dx.doi.org/10.1038/s41467-022-33212-0>.

1064

1065 [52] Yue Hu, Xi Xi, et al. “SCeQTL: an R package for identifying eQTL from single-cell parallel  
1066 sequencing data”. In: *BMC Bioinformatics* 21.1 (May 2020). ISSN: 1471-2105. DOI: [10.1186/s12859-020-3534-6](https://doi.org/10.1186/s12859-020-3534-6). URL: <http://dx.doi.org/10.1186/s12859-020-3534-6>.

1067

1068 [53] Gao Wang, Abhishek Sarkar, et al. “A Simple New Approach to Variable Selection in Re-  
1069 gression, with Application to Genetic Fine Mapping”. In: *Journal of the Royal Statistical  
1070 Society Series B: Statistical Methodology* 82.5 (July 2020), 1273–1300. ISSN: 1467-9868. DOI:  
1071 [10.1111/rssb.12388](https://doi.org/10.1111/rssb.12388). URL: <http://dx.doi.org/10.1111/rssb.12388>.

1072 [54] Lee J. Cronbach and Noreen Webb. “Between-class and within-class effects in a reported  
1073 aptitude \* treatment interaction: Reanalysis of a study by G. L. Anderson”. In: *Journal of  
1074 Educational Psychology* 67.6 (1975), pp. 717–724. DOI: [10.1037/0022-0663.67.6.717](https://doi.org/10.1037/0022-0663.67.6.717).

1075 [55] Alkes L. Price, Agnar Helgason, et al. “Single-Tissue and Cross-Tissue Heritability of Gene  
1076 Expression Via Identity-by-Descent in Related or Unrelated Individuals”. In: *PLoS Genetics*  
1077 7.2 (Feb. 2011). Ed. by Greg Gibson. ISSN: 1553-7404. DOI: [10.1371/journal.pgen.1001317](https://doi.org/10.1371/journal.pgen.1001317).  
1078 URL: <http://dx.doi.org/10.1371/journal.pgen.1001317>.

1079 [56] Shengjie Yang, Yiyuan Liu, et al. “Genome-wide eQTLs and heritability for gene expression  
1080 traits in unrelated individuals”. In: *BMC Genomics* 15.1 (Jan. 2014). ISSN: 1471-2164. DOI:  
1081 [10.1186/1471-2164-15-13](https://doi.org/10.1186/1471-2164-15-13). URL: <http://dx.doi.org/10.1186/1471-2164-15-13>.

1082 [57] Andrey A. Shabalin. “Matrix eQTL: ultra fast eQTL analysis via large matrix operations”.  
1083 In: *Bioinformatics (Oxford, England)* 28.10 (May 15, 2012), pp. 1353–1358. ISSN: 1367-4811.  
1084 DOI: [10.1093/bioinformatics/bts163](https://doi.org/10.1093/bioinformatics/bts163).

1085 [58] R. J. Simes. “An improved Bonferroni procedure for multiple tests of significance”. In: *Biometrika*  
1086 73.3 (1986), pp. 751–754. ISSN: 0006-3444, 1464-3510. DOI: [10.1093/biomet/73.3.751](https://doi.org/10.1093/biomet/73.3.751). URL:  
1087 <https://academic.oup.com/biomet/article-lookup/doi/10.1093/biomet/73.3.751>  
1088 (visited on 04/29/2021).

1089 [59] Patrick Rubin-Delanchy and Nicholas A. Heard. *A test for dependence between two point*  
1090 *processes on the real line*. 2014. DOI: [10.48550/ARXIV.1408.3845](https://doi.org/10.48550/ARXIV.1408.3845). URL: <https://arxiv.org/abs/1408.3845>.

1091 [60] Douglas Bates, Martin Mächler, et al. “Fitting Linear Mixed-Effects Models Using lme4”. In:  
1092 *Journal of Statistical Software* 67.1 (2015), pp. 1–48. DOI: [10.18637/jss.v067.i01](https://doi.org/10.18637/jss.v067.i01).

1093 [61] Yoav Benjamini and Yosef Hochberg. “Controlling the False Discovery Rate: A Practical and  
1094 Powerful Approach to Multiple Testing”. In: *Journal of the Royal Statistical Society Series B: Statistical*  
1095 *Methodology* 57.1 (Jan. 1995), 289–300. ISSN: 1467-9868. DOI: [10.1111/j.2517-6161.1995.tb02031.x](https://doi.org/10.1111/j.2517-6161.1995.tb02031.x). URL: <http://dx.doi.org/10.1111/j.2517-6161.1995.tb02031.x>.

1096 [62] Heng Li, Bob Handsaker, et al. “The Sequence Alignment/Map format and SAMtools”. In:  
1097 *Bioinformatics* 25.16 (June 2009), 2078–2079. ISSN: 1367-4803. DOI: [10.1093/bioinformatics/btp352](https://doi.org/10.1093/bioinformatics/btp352). URL: <http://dx.doi.org/10.1093/bioinformatics/btp352>.

1098 [63] Christopher C Chang, Carson C Chow, et al. “Second-generation PLINK: rising to the chal-  
1099 lenge of larger and richer datasets”. In: *GigaScience* 4.1 (Feb. 2015). ISSN: 2047-217X. DOI:  
1100 DOI: [10.1186/s13742-015-0047-8](https://doi.org/10.1186/s13742-015-0047-8). URL: <http://dx.doi.org/10.1186/s13742-015-0047-8>.

1101 [64] S. T. Sherry. “dbSNP: the NCBI database of genetic variation”. In: *Nucleic Acids Research*  
1102 29.1 (Jan. 2001), 308–311. ISSN: 1362-4962. DOI: [10.1093/nar/29.1.308](https://doi.org/10.1093/nar/29.1.308). URL: <http://dx.doi.org/10.1093/nar/29.1.308>.

1103

1104

1105

1106

1107 [65] Ani Manichaikul, Josyf C. Mychaleckyj, et al. “Robust relationship inference in genome-wide  
1108 association studies”. In: *Bioinformatics* 26.22 (Oct. 2010), 2867–2873. ISSN: 1367-4803. DOI:  
1109 [10.1093/bioinformatics/btq559](https://doi.org/10.1093/bioinformatics/btq559). URL: <http://dx.doi.org/10.1093/bioinformatics/btq559>.

1111 [66] Sayantan Das, Lukas Forer, et al. “Next-generation genotype imputation service and meth-  
1112 ods”. In: *Nature Genetics* 48.10 (Aug. 2016), 1284–1287. ISSN: 1546-1718. DOI: [10.1038/ng.3656](https://doi.org/10.1038/ng.3656). URL: <http://dx.doi.org/10.1038/ng.3656>.

1114 [67] Adam Auton, Gonçalo R. Abecasis, et al. “A global reference for human genetic variation”.  
1115 In: *Nature* 526.7571 (Sept. 2015), 68–74. ISSN: 1476-4687. DOI: [10.1038/nature15393](https://doi.org/10.1038/nature15393). URL:  
1116 <http://dx.doi.org/10.1038/nature15393>.

1117 [68] Zachary R. McCaw, Jacqueline M. Lane, et al. “Operating characteristics of the rank-based  
1118 inverse normal transformation for quantitative trait analysis in genome-wide association stud-  
1119 ies”. In: *Biometrics* 76.4 (Jan. 2020), 1262–1272. ISSN: 1541-0420. DOI: [10.1111/biom.13214](https://doi.org/10.1111/biom.13214).  
1120 URL: <http://dx.doi.org/10.1111/biom.13214>.

1121 [69] Heather J. Zhou, Lei Li, et al. “PCA outperforms popular hidden variable inference methods  
1122 for molecular QTL mapping”. In: *Genome Biology* 23.1 (Oct. 2022). ISSN: 1474-760X. DOI:  
1123 [10.1186/s13059-022-02761-4](https://doi.org/10.1186/s13059-022-02761-4). URL: <http://dx.doi.org/10.1186/s13059-022-02761-4>.

1124 [70] Gabriel E. Hoffman and Eric E. Schadt. “variancePartition: Interpreting drivers of variation  
1125 in complex gene expression studies”. In: *BMC Bioinformatics* 17 (483 2016). DOI: [10.1186/s12859-016-1323-z](https://doi.org/10.1186/s12859-016-1323-z).

1127 [71] Buhm Han and Eleazar Eskin. “Random-Effects Model Aimed at Discovering Associations in  
1128 Meta-Analysis of Genome-wide Association Studies”. In: *The American Journal of Human  
1129 Genetics* 88.5 (May 2011), 586–598. ISSN: 0002-9297. DOI: [10.1016/j.ajhg.2011.04.014](https://doi.org/10.1016/j.ajhg.2011.04.014).  
1130 URL: <http://dx.doi.org/10.1016/j.ajhg.2011.04.014>.

1131 [72] Daniel Ho, Kosuke Imai, et al. “Matching as Nonparametric Preprocessing for Reducing Model  
1132 Dependence in Parametric Causal Inference”. In: *Political Analysis* 15 (2007), pp. 199–236.

1133 [73] Christian Benner, Chris C.A. Spencer, et al. “FINEMAP: efficient variable selection us-  
1134 ing summary data from genome-wide association studies”. In: *Bioinformatics* 32.10 (Jan.  
1135 2016), pp. 1493–1501. ISSN: 1367-4803. DOI: [10.1093/bioinformatics/btw018](https://doi.org/10.1093/bioinformatics/btw018). eprint:  
1136 [https://academic.oup.com/bioinformatics/article-pdf/32/10/1493/49019673/bioinformatics\\_32\\_10\\_1493.pdf](https://academic.oup.com/bioinformatics/article-pdf/32/10/1493/49019673/bioinformatics_32_10_1493.pdf). URL: <https://doi.org/10.1093/bioinformatics/btw018>.

1137 1138

1139 [74] Farhad Hormozdiari, Martijn van de Bunt, et al. “Colocalization of GWAS and eQTL Signals  
1140 Detects Target Genes”. In: *The American Journal of Human Genetics* 99.6 (Dec. 2016),  
1141 1245–1260. ISSN: 0002-9297. DOI: [10.1016/j.ajhg.2016.10.003](https://doi.org/10.1016/j.ajhg.2016.10.003). URL: <http://dx.doi.org/10.1016/j.ajhg.2016.10.003>.

1142

1143 [75] Alvaro N. Barbeira, Rodrigo Bonazzola, et al. “Exploiting the GTEx resources to decipher  
1144 the mechanisms at GWAS loci”. In: *Genome Biology* 22.1 (Jan. 2021). ISSN: 1474-760X. DOI:  
1145 [10.1186/s13059-020-02252-4](https://doi.org/10.1186/s13059-020-02252-4). URL: <http://dx.doi.org/10.1186/s13059-020-02252-4>.

1146 [76] Ruma Banerjee and Cheng-Gang Zou. “Redox regulation and reaction mechanism of human  
1147 cystathionine-beta-synthase: a PLP-dependent hemesensor protein”. In: *Archives of Biochem-  
1148 istry and Biophysics* 433.1 (Jan. 1, 2005), pp. 144–156. ISSN: 0003-9861. DOI: [10.1016/j.abb.2004.08.037](https://doi.org/10.1016/j.abb.2004.08.037).

1149

1150 [77] J. P. Kraus, J. Oliveriusová, et al. “The human cystathionine beta-synthase (CBS) gene:  
1151 complete sequence, alternative splicing, and polymorphisms”. In: *Genomics* 52.3 (Sept. 15,  
1152 1998), pp. 312–324. ISSN: 0888-7543. DOI: [10.1006/geno.1998.5437](https://doi.org/10.1006/geno.1998.5437).

1153 [78] Edith Wilson Miles and Jan P. Kraus. “Cystathionine beta-synthase: structure, function,  
1154 regulation, and location of homocystinuria-causing mutations”. In: *The Journal of Biological  
1155 Chemistry* 279.29 (July 16, 2004), pp. 29871–29874. ISSN: 0021-9258. DOI: [10.1074/jbc.R400005200](https://doi.org/10.1074/jbc.R400005200).

1156

1157 [79] Angata T, Hayakawa T, et al. “Discovery of Siglec-14, a novel sialic acid receptor undergoing  
1158 concerted evolution with Siglec-5 in primates.” In: *FASEB Journal : Official Publication of  
1159 the Federation of American Societies for Experimental Biology* 20.12 (Oct. 1, 2006), pp. 1964–

1160 1973. ISSN: 0892-6638, 1530-6860. DOI: [10.1096/fj.06-5800com](https://doi.org/10.1096/fj.06-5800com). URL: <https://europepmc.org/article/MED/17012248> (visited on 04/02/2021).

1161

1162 [80] Erwin Goldberg, Edward M. Eddy, et al. “LDHC THE ULTIMATE TESTIS SPECIFIC  
1163 GENE”. In: *Journal of andrology* 31.1 (2010), pp. 86–94. ISSN: 0196-3635. DOI: [10.2164/jandrol.109.008367](https://doi.org/10.2164/jandrol.109.008367). URL: <https://www.ncbi.nlm.nih.gov/pmc/articles/PMC2915756/>  
1164 (visited on 04/02/2021).

1165

1166 [81] B. J. Strober, R. Elorbany, et al. “Dynamic genetic regulation of gene expression during  
1167 cellular differentiation”. In: *Science* 364.6447 (June 28, 2019), pp. 1287–1290. ISSN: 0036-  
1168 8075, 1095-9203. DOI: [10.1126/science.aaw0040](https://doi.org/10.1126/science.aaw0040). URL: <https://science.sciencemag.org/content/364/6447/1287> (visited on 04/26/2021).

1169